Geophysics Open File Report No. 25
Geoscience Department
New Mexico Tech
Socorro, NM 87801

A STUDY OF POISSON'S RATIO IN THE UPPER CRUST IN THE SOCORRO, NEW MEXICO, AREA

by

John J. Fender

Submitted in partial
fulfillment
of
the requirement
of
Geophysics 590
and the
Master's Degree Program
at
New Mexico Institute
of
Mining and Technology

September, 1978

The research described in this paper was sponsored jointly by the National Science Foundation (Grant EAR77-23166) and the New Mexico Energy Institute - New Mexico State University (Grant EI-177-2312).

Table of Contents

Acknowledgements

The author wishes to thank Dr. Allan Gutjahr and Eric Rinehart for their help with the statistical and computer oriented problems encountered in this study. Sincere appreciation is extended to Jim Johnston, Mark Frishman, Scott Frishman, Roger Ward, and Eric Rinehart for their efforts in data acquisition and reduction. The author is particularly thankful to Dr. Allan Sanford for his helpful suggestions and comments on all aspects of this research. Particular appreciation is extended to the author's advisor, Dr. John Schlue, whose quick and thorough editing, advice, and overall availability made the completion of this paper possible.

I. Introduction

The purpose of this study was to determine an average Poisson's ratio in the upper crust (<15 km) for the local Socorro region using body wave arrivals from 294 located microearthquakes, and to obtain a spatial distribution of Poisson's ratio using information gleaned from the microearthquake locations. The determination and location of areas with anomalously high Poisson's ratio was of particular interest in this study as these segments of the crust may contain partially molten material.

Poisson's ratio (ν) is a dimensionless quantity representing the ratio of the fractional change in length to the fractional change in diameter in a cylindercal volume of material subjected to a tensional or compressional force, such as the transmission of seismic energy through rock. Since core samples of rock for the entire are of investigation were unavailable, an alternate means for obtaining Poisson's ratio was necessary. The method employed in this study used the arrival times of the P (compressional wave) and S (shear wave) phases and the S-P time intervals (see Figure 1). Note that the plot of S-P intervals versus P arrival times gives a straight line with a slope of $(\frac{\alpha}{\beta}-1)$ which appears in the relation:

$$S-P = (P-O)(\frac{\alpha}{\beta}-1), \qquad (1)$$

where S = S-wave arrival time,
P = P-wave arrival time,
O = Origin time of the microearthquake,
α = P-wave velocity, and
β = S-wave velocity.

Equation 1 may be derived from the definition of the S-P interval, given by:

$$S\text{-}P = \frac{D}{\beta} - \frac{D}{\alpha}, \qquad (1a)$$

where D = distance from the earthquake hypocenter to a receiving seismograph station, and may be written as: $D = (P\text{-}O)\alpha$.

Poisson's ratio may then be calculated using the relation:

$$\nu = \frac{(\frac{\alpha^2}{\beta^2} - 2)}{2(\frac{\alpha^2}{\beta^2} - 1)}, \qquad (2)$$

given by Bullen (1963, page 213). The value of Poisson's ratio may vary between 0 and ½ for different materials but usually is in the neighborhood of ¼ (Nettleton, 1940). The cases where ν is 0 and ½ correspond to a perfectly rigid solid and a perfect liquid, respectively. Poisson's ratio thus provides a measure of the general characteristics of a material, which may be utilized to detect the shallow (<10 km) magma bodies in the Socorro area proposed by Sanford and others (1977), Shuleski (1977), Caravella (1976), Johnston (1978), and Wallace (1978).

II. Geologic Setting

The area of study lies within the Rio Grande rift, in central New Mexico, approximately 120 km south-southwest of Albuquerque. The Rio Grande rift is a major extensional structure formed by east-west tension begining about 25 to 29 m.y. ago and continuing to the present (Chapin and Seager, 1975). The rift is composed of a series of en echelon structural depressions having raised margins and a general northern trend. The rift extends from southern New Mexico into central Colorado, and penetrates the southern Rocky Mountains of northern New Mexico and southern Colorado. The rift lies between the Colorado Plateau and Great Plains in central New Mexico, and merges to the south in a complicated manner with the Basin and Range Province (see Figure 2). The area of investigation encompasses a portion of the Rio Grande rift which has been further modified by intergraben horsts believed to be 9 to 10 m.y. old, suggesting relatively recent crustal structure activity (Chapin and Seager, 1975). Figure 3 shows the general physiographic features of the area of study, where intergraben horsts appear as the Socorro-Lemitar and Chupadera mountains separating the La Jencia and Socorro basins.

A large amount of evidence indicates that volcanic activity accompanied formation of the rift. Several overlapping calderas have been mapped in the Socorro area and are believed

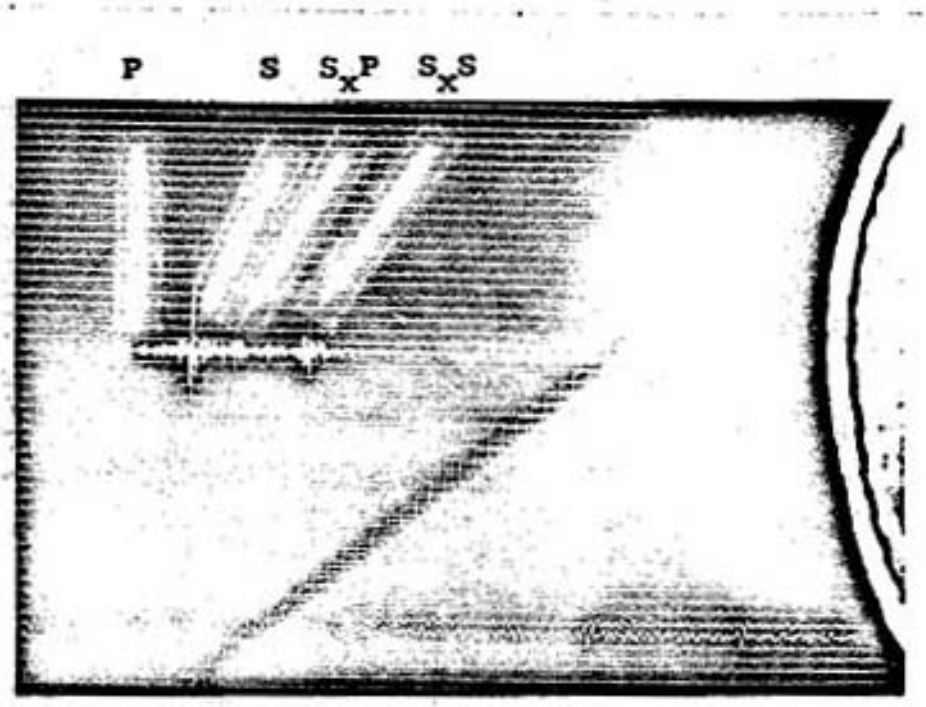

Figure 1. Example of microearthquake used in this study. This event was recorded at seismic station CC on February 19, 1976, and shows the P and S wave arrivals as well as two reflection phases believed to be associated with a deep magma body whose upper surface lies between 18 and 20 km below the area of study. The S-P interval is obtained by subtracting the P arrival time from the S arrival time.

to be the source of voluminous ashflow eruptions which deposited the widespread tuff sheets that cap the Datil-Mogollon volcanic pile. K-Ar dates on these volcanic rocks indicate periods of magmatism at 27-20 m.y., 12-7 m.y. and 4 m.y. ago (Chapin et al., 1978). Early volcanism had basaltic andesites

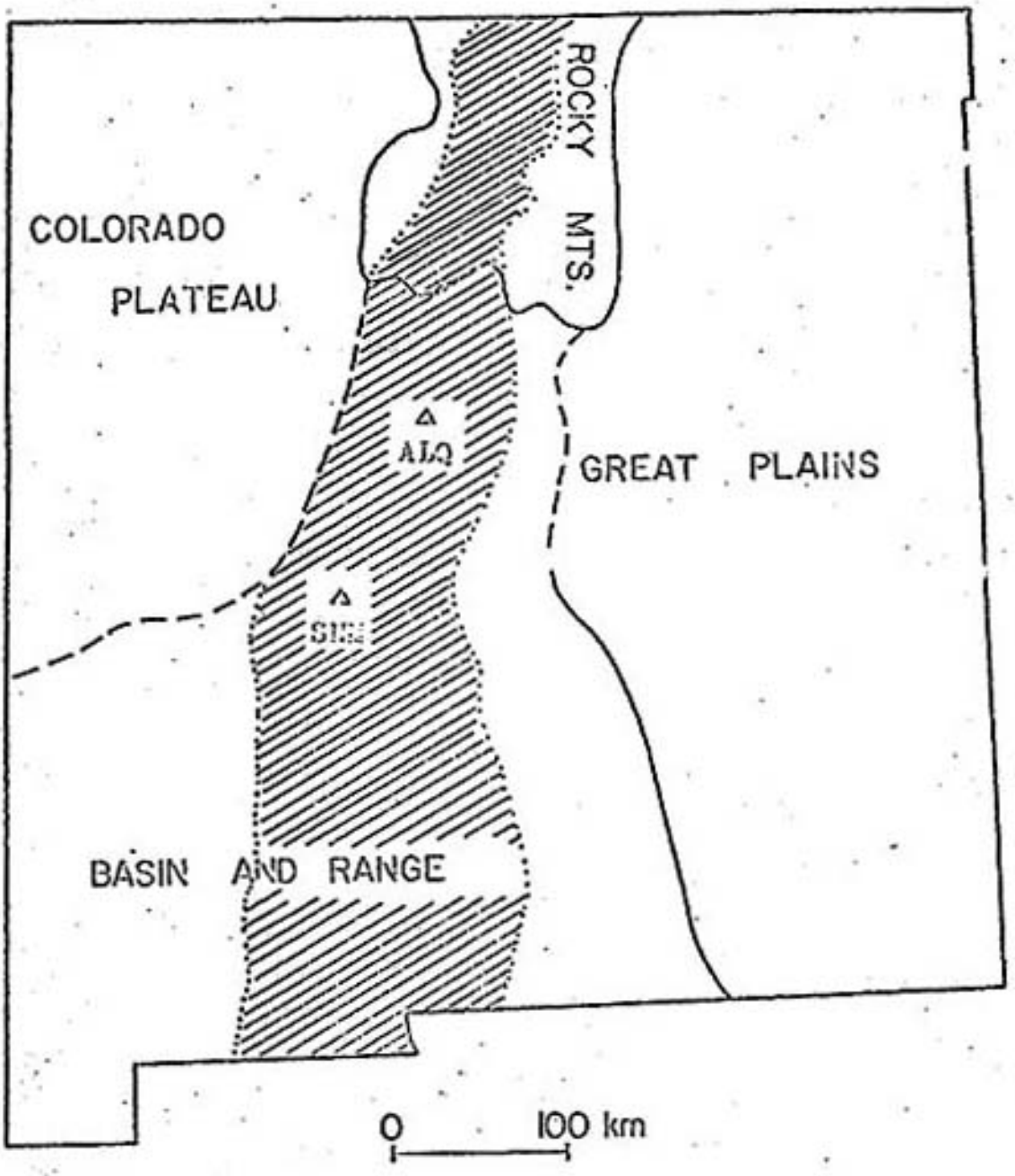

Figure 2. Physiographic provinces in New Mexico. The Rio Grande Rift is shaded (after Toppozada, 1974).

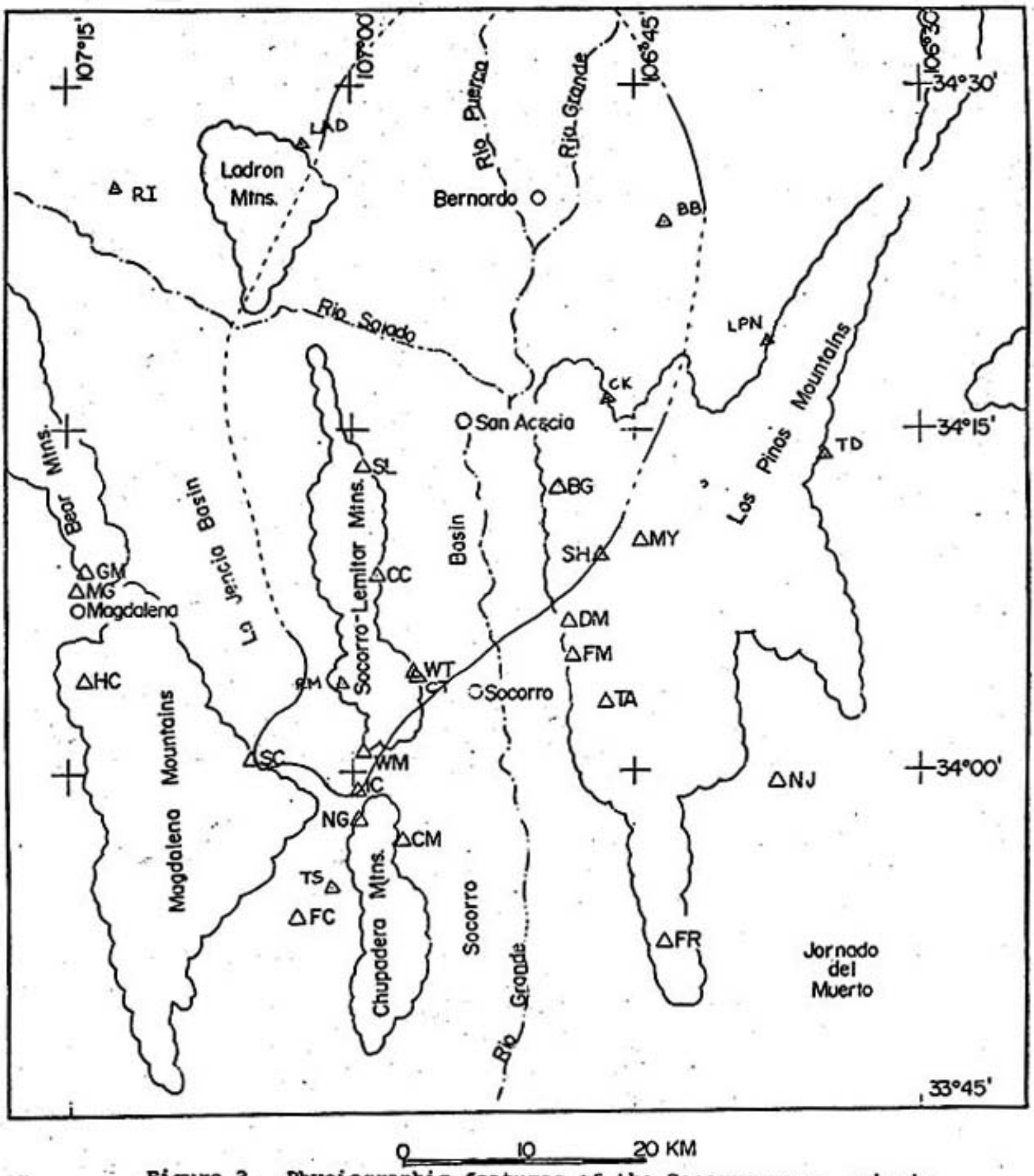

Figure 3. Physiographic features of the Socorro area, seismic station locations, and outline of the deep (18 km) magma body (from Rinehart, 1978).

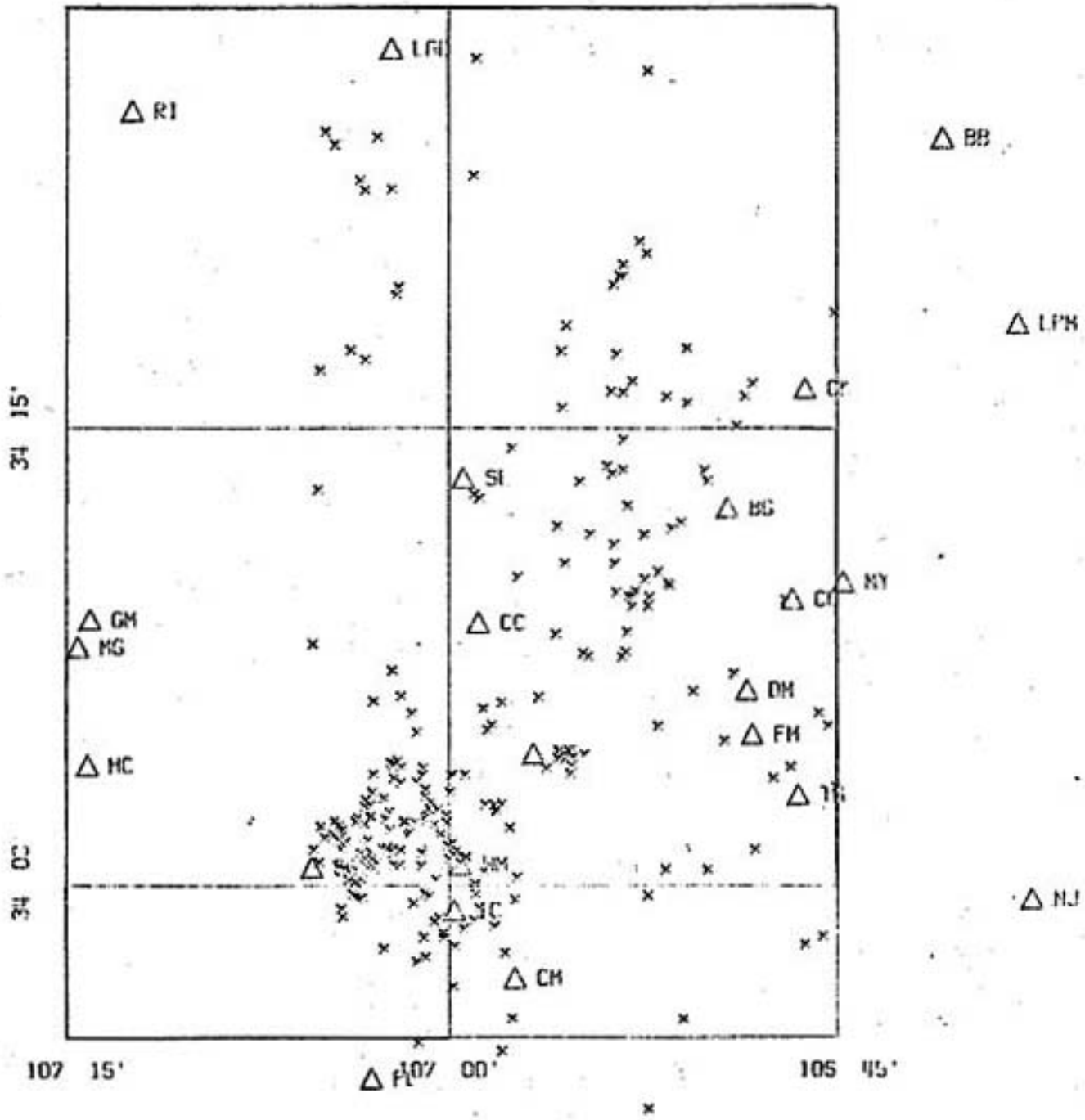

Figure 4. Map showing the epicentral distribution of the microearthquakes used in this study. The 'x' marks represent individual events.

associated with it, while true basalts dominated the flows of very recent age in the Socorro area.

Evidence supporting current activity in and around the rift includes a ribbon of high heat flow (>2.5 HFU) which is roughly coincident with thermal springs occurring along the western margin of the rift (Reiter et al., 1975), a high rate of surface uplift, with a maximum average rate of 6.1 mm per year, approximately 23 km north of Socorro (Reilinger and Oliver, 1976), high microearthquake activity and microearthquakes occurring in swarms. (The epicentral distribution of microearthquakes used in this study is shown in Figure 4.) The hottest and largest thermal springs are located in the southern end of the Socorro-Lemitar mountains where high temperature gradients (maximum, 241°C/km) and heat flows (maximum, 11.7 HFU) have been obtained from boreholes within the Socorro Mountain block (Reiter and Smith, 1977).

An extensive magma body whose upper surface is located between 18 and 20 km in depth has been defined using reflection phases appearing in many microearthquake codas (Rinehart, 1976). The outline of the deep magma body is shown in Figure 3, where dotted lines indicate boundaries where more data are required to map them accurately. The body appears to be thin (approximately 1 to 2 km in vertical thickness) and elongate, and has a general north-south trend (Sanford et al., 1977). The upper surface of the magma body is relatively flat with a slight northward dip of two to three degrees (Rinehart, 1978). The

possibility that this deep magma body serves as a source of the proposed shallower magma bodies is at present unresolved.

III. Previous Studies of Poisson's Ratio in the Rio Grande Rift

A study of Poisson's ratio (ν) was conducted in the Rio Grande rift, between Albuquerque and Socorro, New Mexico by Kiet Sakdejayont (1974). The ratio of P-wave velocity to S-wave velocity was examined using the data obtained from 32 well-recorded microearthquakes within 45 km of the Socorro seismograph station, SNM. The values of α/β and ν were found to be 1.664 and 0.217 respectively. These comparatively low values were considered to be normal values for the Rio Grande rift by Sakdejayont.

A more recent paper involving the calculation and spatial distribution of Poisson's ratio in the Socorro, New Mexico area was that of Caravella (1976). In this study, data from 50 microearthquakes located in and around the southern margins of the Socorro and La Jencia basins were used. Caravella found an average ν of 0.262 with a standard deviation of 0.034 using a method similar to that employed in this paper. This average Poisson's ratio is about 21% higher than the value obtained by Sakdejayont for crustal rock further north in the rift. One notes however that two standard deviations applied to Caravella's value of ν would include the result obtained by Sakdejayont, and one standard deviation applied to both would probably produce a non-null union (Sakdejayont did not state a standard deviation for his value of ν.). Caravella attributed the possible difference in Poisson's

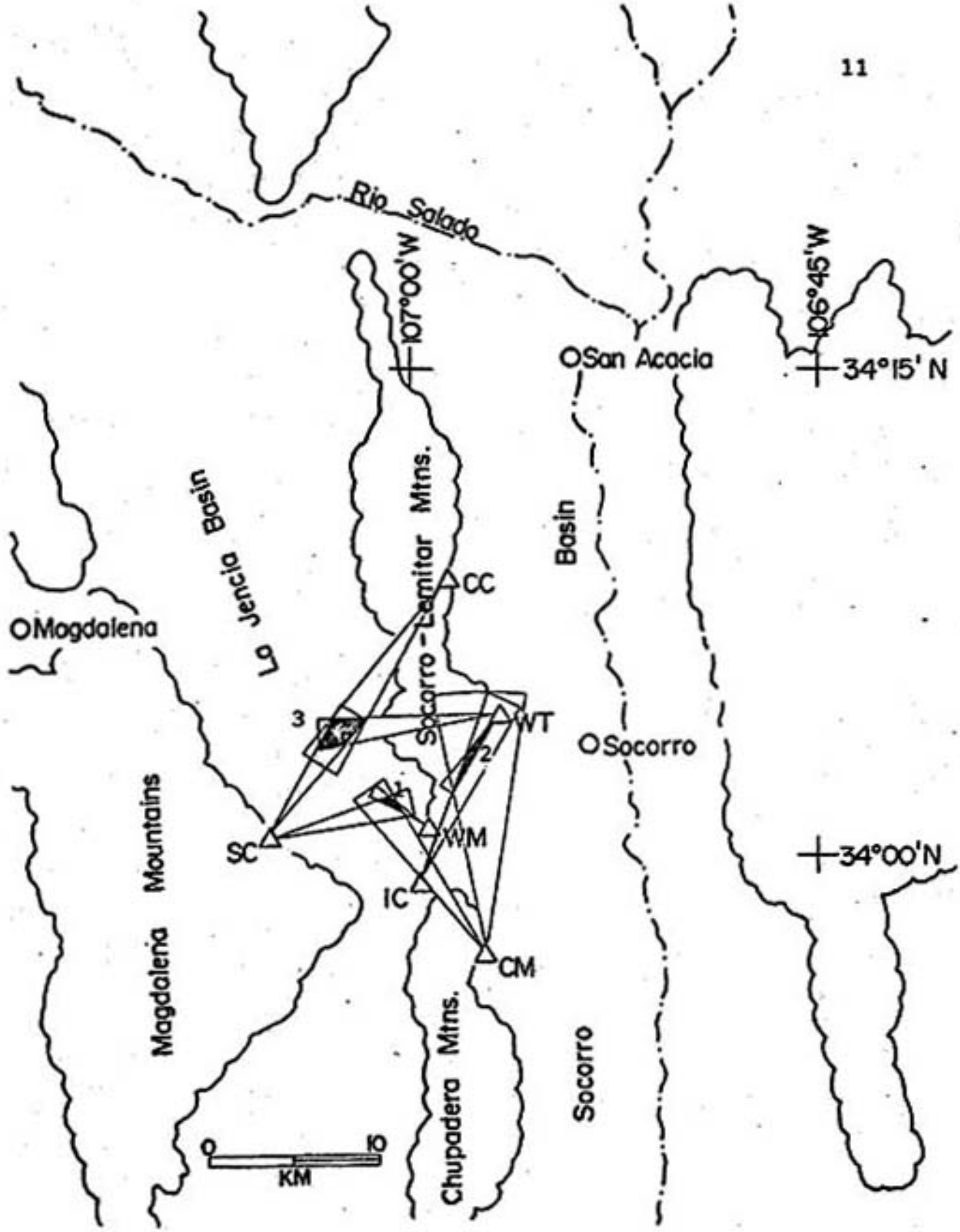

Figure 5. The three areas of anomalous Poisson's ratio proposed by Caravella (1976), obtained using crustal wedge intersections. The areas are: (1) the southern La Jencia basin (ν = 0.292), (2) Socorro Mountain (ν = 0.289), and (3) central La Jencia basin (ν = 0.284).

to a difference in the S-wave velocity for the two areas, 3.30 km/sec. versus 3.49 km/sec. Caravella attempted to determine spatial variations in ν, but found that more data were necessary to resolve such variations in a significant fraction of his study area. His data were sufficient to define three anomalous areas (see Figure 5) having average ν's of 0.292, 0.289 and 0.284. They were: (1) southern La Jencia basin, (2) Socorro Mountain, and (3) central La Jencia basin respectively.

IV. Instrumentation

Microearthquake data used in this study were obtained using two types of portable seismic systems. Throughout the data collection period (April, 1975 to January, 1978) an array of 4 to 6 Sprengnether Instrument Company MEQ-800 analog recording units was deployed. Each MEQ-800 unit consisted of either a Mark Products L4C or Willmore vertical seismometer having natural frequencies of 1.0 and 1.5 Hz respectively, a gain-stable amplifier, a quartz-crystal-controlled timing system, and a smoked-paper helical recorder which operated at a recording speed of 120 mm/min. This basic array was supplimented, starting in April, 1977, with two Sprengnether DR-100 digital recording units equipped with Mark Products L4C vertical seismometers. In addition to these units, a Kinematics PS-1 analog unit, with a recording speed of 150 mm/min., was used to record station LAD which was telemetered via telephone line directly to the campus of New Mexico Institute of Mining and Technology. The MEQ-800 seismographs served as the fundamental source for data, while the PS-1 unit and DR-100 systems were primarily used to improve hypocenter locations by expanding the existing arrays.

During the data collection period, many different arrays were used, and in all, 26 different station locations were occupied (see Figure 3). Table 1 lists these seismograph stations along with their locations and elevations. Elimin-

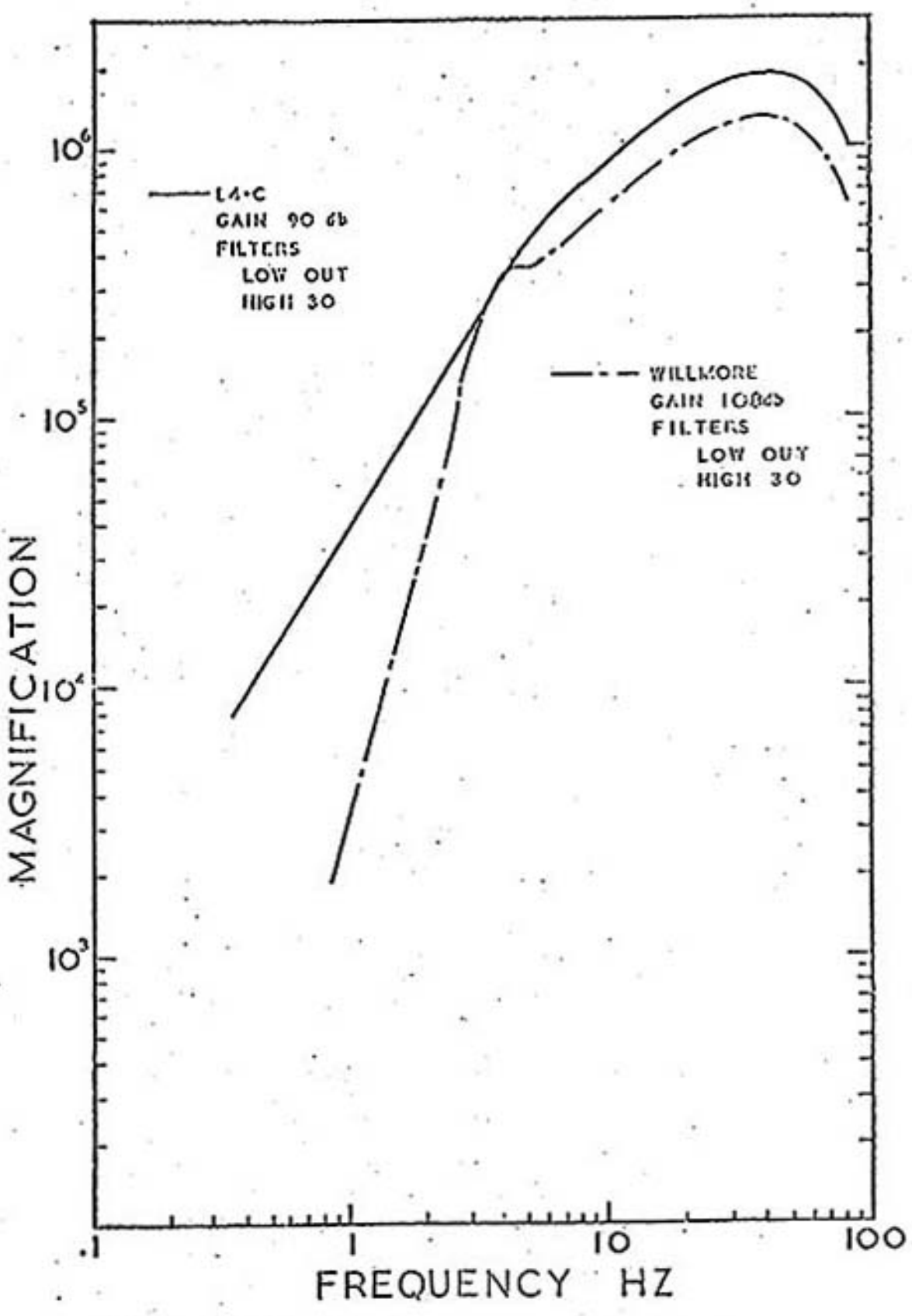

Figure 6. Magnification response curves for the MEQ-800 seismographs. The high-frequency filter is set in the 30 Hz position (adapted from Rinehart, 1976).

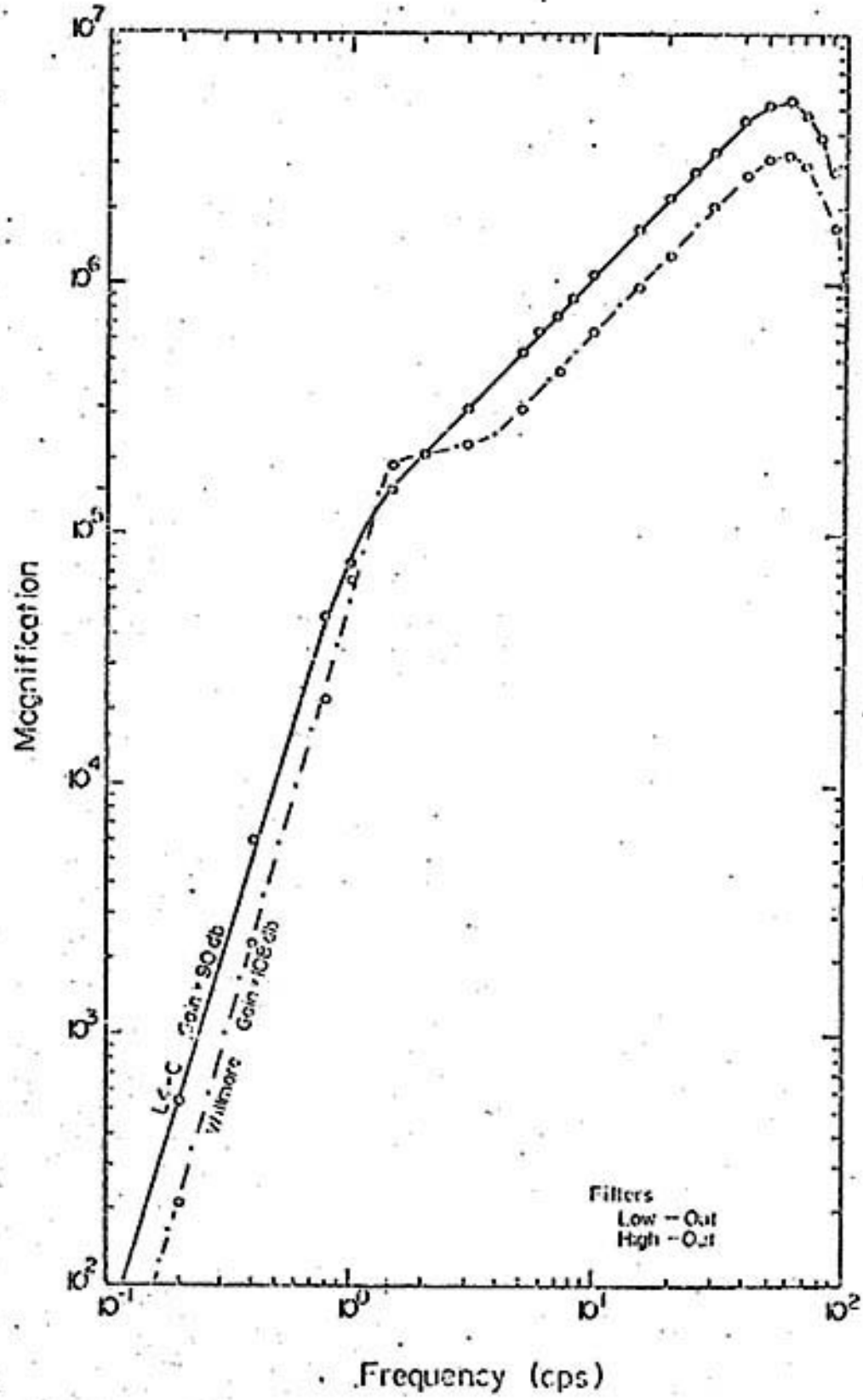

Figure 7. Magnification response curves for the MEQ-800 seismographs. The high-frequency filter is set in the Out position (from Shuleski, 1976).

Table 1. Location of Seismic Stations

Station	Latitude	Longitude	Elevation (m)
BB	34.4090	106.6818	1615
BG	34.2068	106.8205	1516
CC	34.1442	106.9812	1649
CK	34.2725	106.7702	1578
CM	33.9501	106.9576	1640
CU	34.1573	106.7785	1585
DM	34.1075	106.8079	1536
FC	34.8950	107.0504	1850
FM	34.0829	106.8047	1537
FR	33.8745	106.7270	1558
GM	34.1454	107.2345	1945
HC	34.0658	107.2361	2240
IC	33.9870	106.9967	1730
LAD	34.4583	107.0375	1768
LPN	34.3076	106.6336	1737
MG	34.1305	107.2425	2024
MY	34.1667	106.7459	1645
NG	33.9648	106.9933	1730
NJ	33.9924	106.6253	1644
RI	34.4234	107.2075	1530
SC	34.0100	107.0894	2073
SL	34.2234	106.9910	1615
TA	34.0498	106.7751	1558

Table 1. (continued)

Station	Latitude	Longitude	Elevation (m)
TD	34.2339	106.5778	1850
WM	34.0120	106.9929	1673
WT	34.0722	106.9459	1555

ation of atmospheric and man-made noise were two prerequisites for station site selection. All seismograph stations selected rested upon bedrock. In most cases, caves and abandoned mines were used and proved quite satisfactory, but when high background noise levels were encountered, lower gain settings and/or filtering were employed to increase signal to noise ratios.

The MEQ-800 and PS-1 units have gain settings ranging from 60 to 120 db in discrete 6 db increments. Some filtering of the seismic signal was possible for both low frequencies (below 5 or 10 Hz) and high frequencies (above 5, 10, or 30 Hz). For this study, the 30 Hz setting on the high frequency filter was used over 50% of the time and nearly 100% of the time for the noisiest stations (BG, CU, FC, HC, SL, TA, MY). The filtering was necessary to reduce noise generated by wind and small animals. The microearthquake signals were not impaired greatly by this filtering since the MEQ-800 unit still showed good responce at that setting for frequencies around

30 Hz, the dominant frequency of the P arrival (Sanford and Holmes, 1962). The DR-100 systems have gain settings ranging from 78 to 96 db in discrete 6 db intervals with both high and low frequency filtering available. In general, the highest possible gain setting with least filtering was used. For the MEQ-800 systems, this resulted in most of the gain settings falling between 78 and 90 db for the data used in this study. Magnification versus frequency plots are shown in Figures 6 and 7 for the MEQ-800 seismographs, for both types of geophones used, at typical gain and filter settings.

V. Data Collection, Reduction, and Analysis

Section 1

Obtaining accurate times for both the first arrival and S phase was of fundamental importance to this study. Before each recording period (4-6 days in duration), the clocks on all seismographs were either synchronized to WWV-UST (broadcast from Fort Collins, Colorado) or the time difference was noted. Similarly, at the end of the recording period, the clocks were checked for any drift which may have occurred. Any clock drift was assumed to have occurred linearly and timing corrections were made accordingly. Several tests of the linearity of clock drift assumption were made, both in the field and inside a single building or mine where the temperature was essentially constant. Two to three drift measurements were made on each seismograph unit at approximately 8 hour intervals so that any deviation of the clock drift from linearity might be better defined. The tests showed that the maximum divergence from linearity was less than 5%, which would result in a time correction error of less than 0.03 seconds.

The PS-1 and MEQ-800 seismograms were read with a Gaertner traveling microscope, which has a measuring accuracy of approximately 0.005 mm (~0.003 seconds). Tests show that different individuals can read the same record with an accuracy of about 0.04 mm (~0.02 seconds) (Rinehart, personal

communication, 1978). The DR-100 cassette recordings were usually played back on a strip-chart recorder at a rate of ~60 mm per second, allowing a very accurate measurement to be made with the use of a millimeter scale.

The data used in this study consist of three basic measurements: (1) the P arrival times, (2) the S-P intervals, and (3) the distance between minute marks on either side of the onset of an event, all measured in millimeters (see Appendix C). The adjacent distance between minute marks was used when the minute in which the microearthquake arrived was split when taken off the seismograph drum. Times were then calculated in seconds by dividing measurements 1 and 2 by measurement 3 and multiplying by 60. A similar procedure was used to obtain times from the DR-100 records. The P arrival times were then corrected using the clock drift corrections described above. Uncertainties in these times were estimated by repeating the measurements at least three times for each event used.

Section 2

Microearthquake locations were obtained for 294 microearthquakes using a numerical inversion computer program. The crustal model assumed in this iterative inversion program was an isotropic, homogeneous half-space with a P-wave vel-

ocity of 5.80 km/sec. A trial hypocenter was determined using: (1) chord intersections from a circle plot of the S-P intervals for the stations in the array, (2) a Wadati diagram (plot of the S-P intervals versus the P arrival times), and (3) an assumed depth of 7.0 km. The circle plot yielded trial values for the longitude and latitude for the hypocenter, while the Wadati diagram gave an initial estimate of the origin time for the event. The initial value of 7.0 km for the depth was used as it is the average depth of focus for earthquakes occurring in the Socorro area (Sanford, personal communication, 1978). The average depth found for the 294 microearthquakes located in this study was 6.7 km. The computer printouts of the final microearthquake hypocenters are included in an appendix separate from this paper, whereas the measurements used to obtain the locations may be found in Appendix C of this report.

In addition to the crustal parameters, P arrival times and trial hypocenter, the iterative inversion program utilized station corrections which corrected for local changes in velocity that exist in the rock column directly beneath the seismograph stations. The corrections, which varied from 0 to 0.48 seconds, were subtracted from the P arrival times at the onset of the location procedure. A list of the station corrections used in this study may be found in Table 2. An explanation of the two methods used to obtain these

Table 2. Station Corrections.

Station	Correction	Method of Determination
WT	0.00	explosion
CC	-0.11	
SL	-0.11	
GM	-0.11	
IC	-0.38	
RM	-0.44	
NG	-0.35	
CM	-0.42	
SC	-0.48	
DM	-0.11	
FM	-0.22	
BG	-0.22	
CU	-0.17	
WM	-0.32	
RI	-0.38	iterative inversion
MY	-0.12	
HC	-0.33	
FC	-0.47	
TS	-0.47	
TA	-0.15	
BB	-0.18	
CK	-0.22	

corrections is given by Johnston(1978).

The microearthquake location program utilized a weighted least-squares approach given by Aki (1976). The solutions obtained were rated using the following formula:

$$R = \left[\frac{1}{N} \sum_{i=1}^{N} \left(\frac{r_i}{w_i} \right)^2 \right]^{1/2}, \qquad (3)$$

where N = number of stations used in location,
r_i = travel-time residuals (difference between theoretical and actual travel times), and
w_i = a priori uncertainties in the travel-time measurements (0.05 to 0.50 seconds in this study).

The value of R indicates how well the travel-time residuals are minimized within the weighting framework and , when R is close to 1.0, indicates that a solution which is both as good as possible and as good as is necessary has been obtained. (i.e. solutions having an R value close to 1.0 are optimal for the weights assigned the P arrival times for those solutions) Locations with $R \ll 1$ will result in uncertainties in the hypocentral parameters which are unnecessarily large, while solutions with $R \gg 1$ will result in solutions whose hypocentral parameters have unjustifiably small uncertainties. The weights assigned to the P arrival times were dependent upon the background noise levels and the character of P phases observed (impulsive or emergent) on the records. The weight generally assigned to the arrival times was 0.05 seconds, which was obtained by summing the reading and clock

drift correction errors mentioned previously. Of the 294 microearthquakes located, 251 had an R value lying between 0.50 and 1.50, while only 7 earthquakes had values of R greater than 2.50.

Since four unknowns are determined by the location program, at least four P arrival-times (i.e. four stations recording an event) are necessary to obtain a solution. This study includes 75 four-station locations, 121 five-station locations, 77 six-station locations, 17 seven-station locations, and 4 eight-station locations. Having more than four stations usually reduced the uncertainties in the hypocentral parameters. This was of particular importance to this study because the uncertainty in the iterative origin time was used in formulating the weights for the analysis of Poisson's ratio using travel-times.

Section 3

The determination of uncertainties for the measurements used in this study was of particular concern to the author. In order to handle the data collected in a statistical manner, a system for reading the S-P intervals was devised. The procedure consisted of three independent measurements of the S-P time, which was assigned a grade of E, G, or P prior to the first measurement. The criteria for assigning these three grades were as follows:

E: Very sharp P and S phases. No noise obscuring either arrival.

G: Some noise affecting the P and/or S phases, i.e. less well-defined arrivals but P and S picks are obvious.

P: Any combination of noise, clipping and "white-out" (found only on the strongest microearthquakes), or emergent character of P and/or S phases, making S-P time subjective but not unreasonable.

Any S-P interval which was split when the record was taken of the seismograph drum was assigned a grade of P. Examples of each of the above types of S-P intervals encountered in this study are shown in Figures 8a, 8b, and 8c. The two basic properties of amplitude and frequency change in the seismogram trace were used predominantly to pick the S phase, the S-wave generally having the largest amplitude and lower frequency content. The mean and standard deviation were calculated for each trio of S-P measurements, which were then grouped according to their assigned grade. Fourty-three percent of the S-P intervals measured were graded E, and were found to have an average standard deviation of 0.007 seconds. S-P intervals receiving a grade of G comprised about 36% of the readings and had an average standard deviation of 0.009 seconds. The remaining S-P measurements received a grade of P and had an average standard deviation of 0.012 seconds. These small average standard deviations appear to represent the

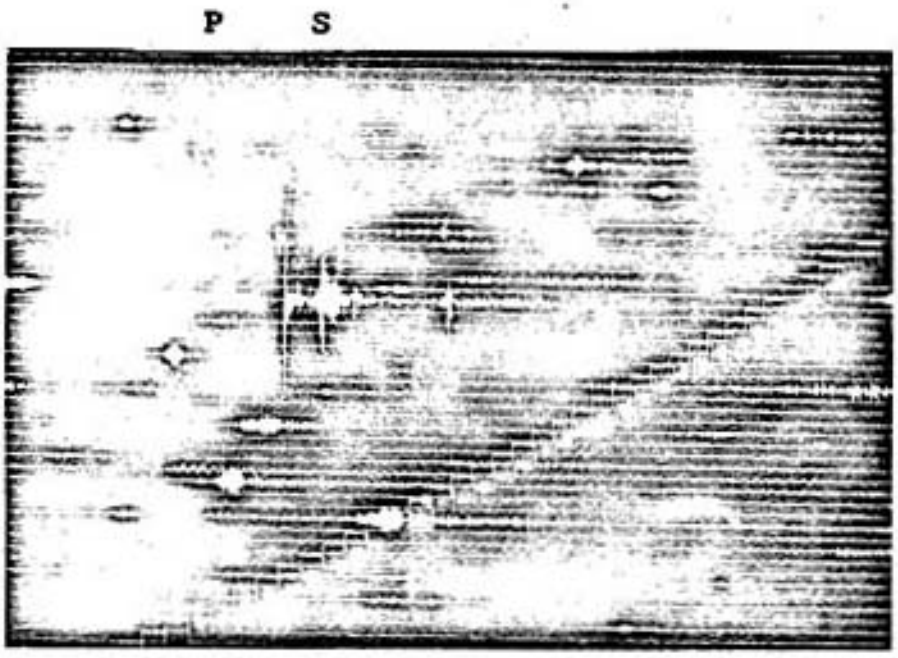

Figure 8a. Example of microearthquake having an S-P interval that received a grade of E. Both the P and S phase exhibit sharp, impulsive onsets. Event was recorded at station WM on February 19,1976 at 00:08.

inaccuracy introduced by the traveling microscope, which has been described previously. Although a small increase in the standard deviation was found to exist as the quality of the S-P interval decreased, the overall error associated with any S-P measurement is small when compared with the uncertainties in the P arrival time. This result indicates consistency in the picking of the P and S arrivals, but not necessarily the error associated with the S-P determination. (i.e. The ability to pick the same breaks on the seismogram

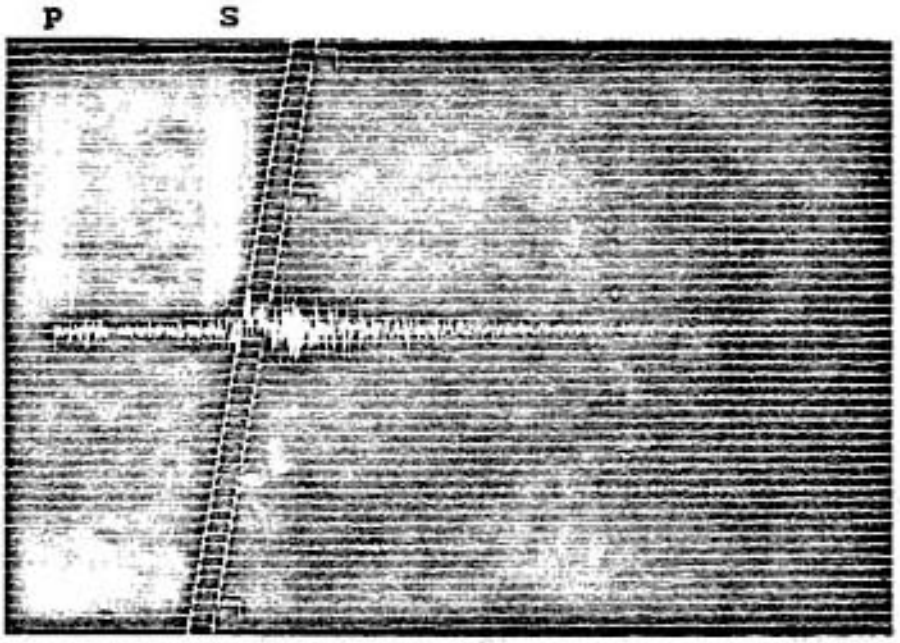

Figure 8b. Microearthquake recorded at station SC on February 19, 1976 at 00:54. The S-P interval for this event received a grade of G. The P pick is obvious while the S arrival is somewhat subjective.

for the arrivals of the P and S waves does not reflect upon the correctness of the resulting S-P interval, as one might consistently pick the P and/or S arrival incorrectly.) For this reason, the uncertainties assigned to the S-P values were the sum of the P arrival-time uncertainty and the standard deviation found for the S-P time. These uncertainties were then used in the Wadati diagram analysis as the weights in the weighted least-squares linear regression.

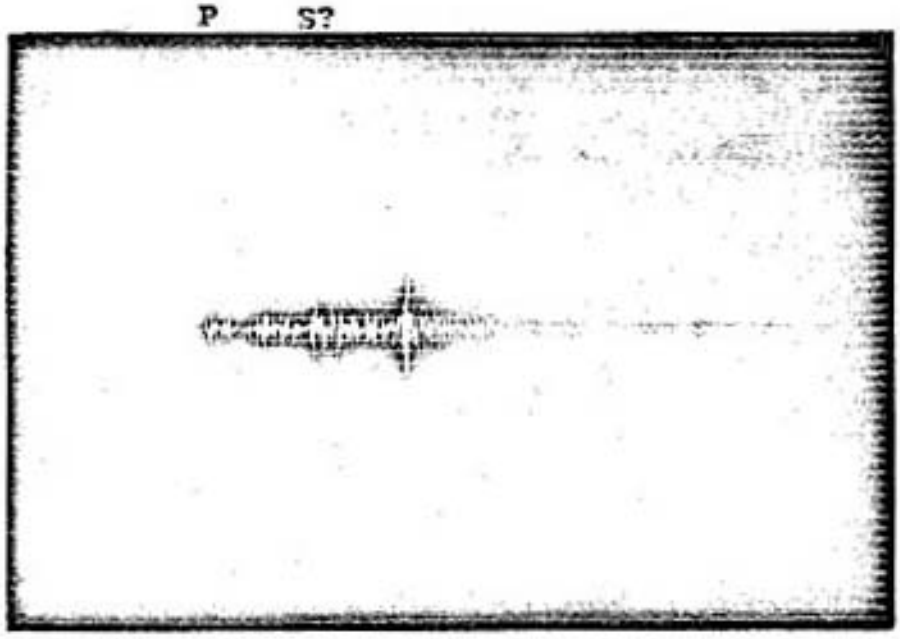

Figure 8c. Microearthquake recorded at station IC on March 23, 1976 at 12:53. The S phase pick is highly subjective for this event, and although the P phase may be easily found, the S-P interval may be subject to a large error if the incorrect S arrival is chosen. For this reason, the grade assigned to the S-P for this event was P.

The weights employed in the travel-time analysis were the sum of the uncertainties in the iterative origin time, S-P interval and the P arrival-time. (The sum of these uncertainties was used, as the measurement and determination of the P arrival, S-P interval, and iterative origin time are not independent.)

Section 4

The procedures used to calculate Poisson's ratio involved the use of the P arrival-times, S-P intervals, distances from seismic stations to earthquake epicenters, azimuths from stations to earthquake locations, and earthquake origin times. The P arrival-times and S-P intervals were obtained directly from the seismograph records, as outlined in Sections 1 and 2, while the remaining information was calculated by the location program discussed in Section 3. The origin-times and P arrival-times were used to determine the P travel-times (P travel-time = P arrival-time - iterative origin-time), which completed the data needed for this study.

The analysis used to obtain an average value of V for the upper crust in the area of study utilized only the P arrival-times, S-P intervals and the uncertainties associated with their determination. Of the 294 microearthquakes located, 277 were deemed suitable for this analysis. The reasons for eliminating a microearthquake solution from the calculations were : (1) poor hypocentral determination caused by an inadequate seismic station distribution about the event and (2) an insufficient number (<4) of readable S-P intervals due to saturation and/or clipping of seismic signals and/or apparent absence of the S phase on a number of the seismogragh records used to locate the event. A weighted least-squares linear regression was used for each of the

277 Wadati plots constructed. The resulting slopes found for the lines determined by this procedure were then used to calculate Poisson's ratio, using equations 1 and 2.

The method of weighted least-squares was employed because this approach allowed the incorporation of the previously determined uncertainties found for the measurements. The quantity that one desires to minimize in the Wadati weighted least-squares regression is :

$$\sum_{i=1}^{N} (a + bx_i - y_i)^2 w_i, \qquad (4)$$

where a = the y-intercept of the fitted line,
b = the slope of the line ($= \frac{\alpha}{\beta} - 1$, where α and β are the velocities of the P and S wave respectively),
x_i = the P arrival-times,
y_i = the S-P intervals,
w_i = the associated uncertainties for the S-P intervals, and
N = the number of points (stations) in the plot.

Expression 4 represents the sum of the squares of the deviations of the data from the weighted least-squares line. To minimize this expression, derivatives with respect to a and b are found and set equal to zero. The resulting two equations are given by :

$$\sum_{i=1}^{N} (a + bx_i - y_i) w_i = 0 \qquad (5)$$

and

$$\sum_{i=1}^{N} (x_i)(a + bx_i - y_i)w_i = 0. \qquad (5a)$$

Equations 5 and 5a may be solved simultaneously for a and b to obtain:

$$a = \frac{\left(\sum_{i=1}^{N} y_i w_i\right)\left(\sum_{i=1}^{N} x_i^2 w_i\right) - \left(\sum_{i=1}^{N} x_i y_i w_i\right)\left(\sum_{i=1}^{N} x_i w_i\right)}{\left(\sum_{i=1}^{N} w_i\right)\left(\sum_{i=1}^{N} x_i^2 w_i\right) - \left(\sum_{i=1}^{N} x_i w_i\right)^2} \qquad (6)$$

and

$$b = \frac{\left(\sum_{i=1}^{N} x_i w_i\right)\left(\sum_{i=1}^{N} y_i w_i\right) - \left(\sum_{i=1}^{N} x_i y_i w_i\right)\left(\sum_{i=1}^{N} w_i\right)}{\left(\sum_{i=1}^{N} x_i w_i\right)^2 - \left(\sum_{i=1}^{N} x_i^2 w_i\right)\left(\sum_{i=1}^{N} w_i\right)} \qquad (6a)$$

Equation 2 may now be rewritten in terms of b, the slope, to get :

$$V = \frac{b^2 - 2b - 1}{2b^2 + 4b} \qquad (2')$$

The degree to which the data fitted the deduced line was ex-

pressed by a correlation coefficient given by :

$$R = \left(\frac{\text{total sum of squares - residual sum of squares}}{\text{total sum of squares}} \right)^{1/2}, \quad (7)$$

which for the Wadati diagrams was :

$$R = \left(\frac{\sum_{i=1}^{N} (y_i - \bar{y})^2 - \sum_{i=1}^{N} (y_i - (a + bx_i))^2}{\sum_{i=1}^{N} (y_i - \bar{y})^2} \right)^{1/2}, \quad (7a)$$

where $\bar{y}$ = the mean of the y_i.

In addition to having a correlation coefficient for the plots, a method for determining the standard deviation of the calculated Poisson's ratios was devised. The method adopted the approximation :

$$\mathrm{Var}(\nu(b)) \approx \left(\frac{d(\nu(b))}{db} \right)^2 \mathrm{Var}(b) , \quad (8)$$

where $\nu(b)$ = Poisson's ratio as a function of slope (equation 2'),

$\frac{d(\nu(b))}{db}$ = the derivative of equation 2' with respect to b, and

Var(b) and Var(ν(b)) are the variances of the slope and Poisson's ratio respectively (Gutjahr, personal communication).

The standard deviation of ν was obtained by taking the square-root of the right-hand side of equation 8.

In order to obtain the variance of the slope in equation 8, a rearrangement of the summations in equation 6a is necessary to isolate the y_i terms. Consider the generalized product of summations:

$$\sum_{i=j}^{N} x_i w_i \sum_{j=1}^{N} y_j w_j = \sum_{i=1}^{N} \sum_{j=1}^{N} x_i w_i y_j w_j = \sum_{j=1}^{N} \sum_{i=1}^{N} x_j y_j w_j w_i . \quad (9)$$

Given the above identity, one can rewrite the numerator of the right-hand side of equation 6a to obtain :

$$\begin{aligned} \text{numerator of } b &= \sum_{j=1}^{N} \left(\sum_{i=1}^{N} x_i w_i \right) w_j y_j - \sum_{j=1}^{N} \left(\sum_{i=1}^{N} w_i \right) x_j y_j w_j \\ &= \sum_{j=1}^{N} \left(\sum_{i=1}^{N} x_i w_i - \sum_{i=1}^{N} w_i x_j \right) w_j y_j , \end{aligned} \quad (10)$$

so that equation 6a becomes :

$$b = \frac{\sum_{j=1}^{N} \left(\sum_{i=1}^{N} x_i w_i - \sum_{i=1}^{N} w_i x_j \right) w_j y_j}{\left(\sum_{i=1}^{N} x_i w_i \right)^2 - \left(\sum_{i=1}^{N} x_i^2 w_i \right) \left(\sum_{i=1}^{N} w_i \right)} . \quad (6a')$$

The variance of the slope may be easily found from equation 6a', and is given by :

$$\text{Var}(b) = \frac{\sum_{j=1}^{N} \left(\sum_{i=1}^{N} x_i w_i - \sum_{i=1}^{N} w_i x_j \right)^2 w_j^2 \text{Var}(y_j)}{\left[\left(\sum_{i=1}^{N} x_i w_i \right)^2 - \sum_{i=1}^{N} x_i^2 w_i \sum_{i=1}^{N} w_i \right]^2} , \quad (11)$$

where $\text{Var}(y_j)$ = the variance of the S-P measurements.

Note that the expression, $w_j^2 \mathrm{Var}(y_j)$, is identically equal to one, since the variance of the y_j's is just the reciprocal of the square of the standard deviations (the w_j's).

The final calculation performed for the Wadati diagram analysis was the determination of weighted least-squares origin-times. These origin times were used to check the reliability of the iterative origin-times generated by the microearthquake location program. Large differences (several seconds) between iterative and weighted least-squares origin-times were occasionally encountered in microearthquake solutions. When a difference of greater than one second was found between origin-times, the data for that plot were excluded from any further analysis. Solutions exhibiting this inconsistency were either solutions for earthquakes falling well outside the array, or were events having all recording stations nearly equidistant from their hypocenters. (A discussion of the latter situation, and its effects upon the inversion problem may be found in the paper by Aki(1976).) The reasons for excluding these earthquakes from the analysis were : (1) the travel-times obtained from the iterative origin-times and P arrival-times for an event were not consistent with any of the S-P measurements for the microearthquake, and (2) when all the recording seismograph stations were equidistant from the earthquake, the corresponding Wadati diagram was very poorly defined, with all the

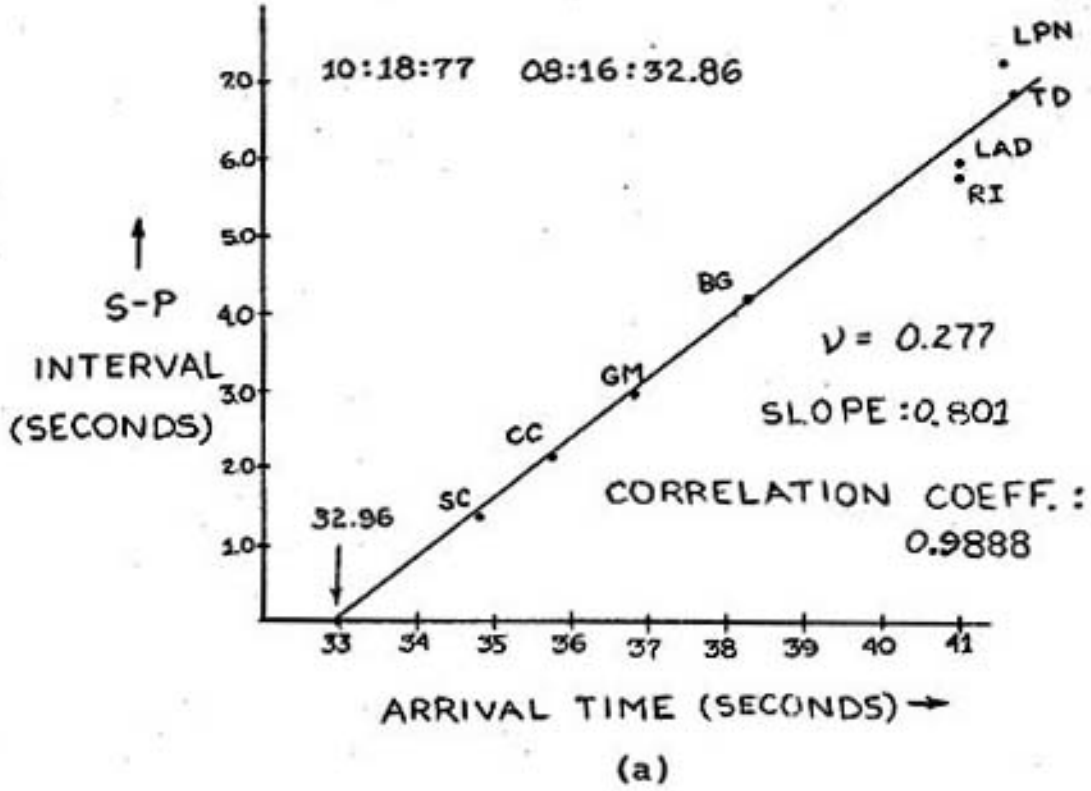

Figure 9. (a) Wadati diagram for an eight station location used in this report. (The weights were all 0.05 sec.)
(b) Travel-time diagram used to obtain V for crustal wedge from station SC.

data plots plotting in essentially the same area. An example of a Wadati diagram used in the above analysis is shown in Figure 9a.

Section 5

The next analysis to be performed was designed to ascertain whether or not plots of S-P intervals versus travel-times could be used to obtain Poisson's ratio (i.e. whether the ratio $\frac{\alpha}{\beta}$ is relatively constant for the study area). The method involved the construction of a single composite plot of all the microearthquake data used in this study. Travel-times were calculated using iterative origin-times from 259 microearthquakes and their associated P arrival-times. The weights employed in the composite plot were obtained by summing the uncertainties in origin-time, P arrival-time and S-P interval for each point in the plot. The results of the analysis were expressed in terms of a correlation coefficient given by equation 12, below :

$$R = \left[\frac{\sum_{i=1}^{N} (y_i - \bar{y})^2 - \sum_{i=1}^{N} (y_i - bt_i)^2}{\sum_{i=1}^{N} (y_i - \bar{y})^2} \right]^{\frac{1}{2}}, \qquad (12)$$

where y_i = the S-P intervals,
$\bar{y}$ = the mean of the y_i's,
b = the slope of the fitted line, and
t_i = the travel-times associated with the S-P intervals.

Section 6

The final segment of the data analysis and reduction involved the determination of spatial variations in Poisson's ratio in the upper crust for the area of study. For a complete description of the technique employed, the reader is directed to the paper by Caravella(1976). Essentially, plots of S-P intervals versus travel-times were constructed for body waves arriving along particular ten degree increments of azimuth about a seismograph station. The principle is represented graphically in Figure 10. A weighted least-squares linear regression was performed for each of the travel-time diagrams which had a minimum of three data points. Poisson's ratio was then calculated, using equations 1 and 2, from the slopes obtained from the linear regressions.

The method of weighted least-squares linear regression, as applied to S-P interval versus travel-time plots, is essentially the same as that employed for the Wadati analysis, although the algebra involved is simplified somewhat. The expression used to calculate the correlation coefficients for the travel-time diagrams is given by equation 12, above. The quantity minimized in this analysis given by:

$$\sum_{i=1}^{N} (bt_i - y_i)^2 w_i \qquad (13)$$

where N is the number of points used in the plot and t_i, y_i, and w_i represent the estimates (measurements or calculations) of the travel-time, S-P interval, and the weight associated with the S-P interval respectively. Thus the travel-time analysis was reduced to the determination of a single variable; the slope of the fitted line through the origin. Values for Poisson's ratio obtained from the slopes were

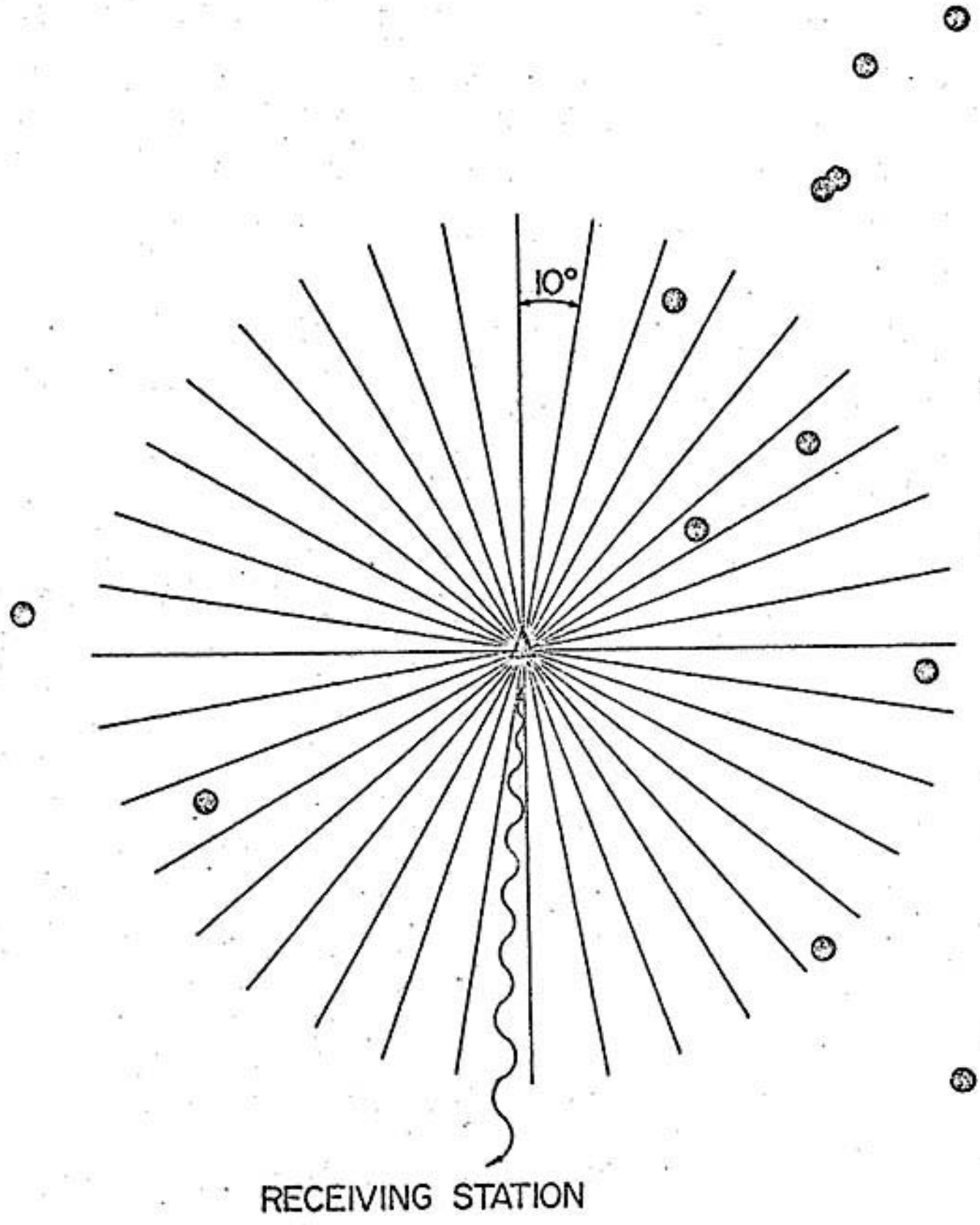

Figure 10. Graphical representation of the technique employed to spatially distribute Poisson's ratio (from Caravella, 1976). Body wave arrivals along ten degree increments of azimuth about a seismograph station are used to form an S-P interval versus travel-time plot. Crustal wedges are then constructed for each plot made.

assigned to the appropriate ten-degree sector of the seismograph station being examined.

To minimize the expression in 13, the derivative with respect to b is found and set equal to zero to obtain:

$$b\sum_{i=1}^{N} t_i^2 w_i - \sum_{i=1}^{N} t_i y_i w_i = 0. \tag{14}$$

the slope is then found to be:

$$b = \frac{\sum_{i=1}^{N} t_i y_i w_i}{\sum_{i=1}^{N} t_i^2 w_i} \tag{15}$$

The approximation given in equation 8 was again employed in the calculation of the standard deviation of Poisson's ratio. The expression used to obtain the variance of the slope for the travel-time plots is:

$$Var(b) = \frac{\sum_{i=1}^{N} t_i^2 w_i^2 Var(y_i)}{\left(\sum_{i=1}^{N} t_i^2 w_i\right)^2}, \tag{16}$$

where again the $w_i^2 Var(y_i)$ term is identically equal to one, as $Var(y_i) = 1/w_i^2$. An example of a travel-time diagram used in this study is shown in Figure 9b. The information obtained by this segment of the study was used to construct crustal wedges having angular widths of of ten degrees and lengths corresponding to the most distant epicenter used in the plot. (see Figure 10) Intersections of crustal wedges exhibiting abnormally high (> 0.275) Poisson's ratios were used

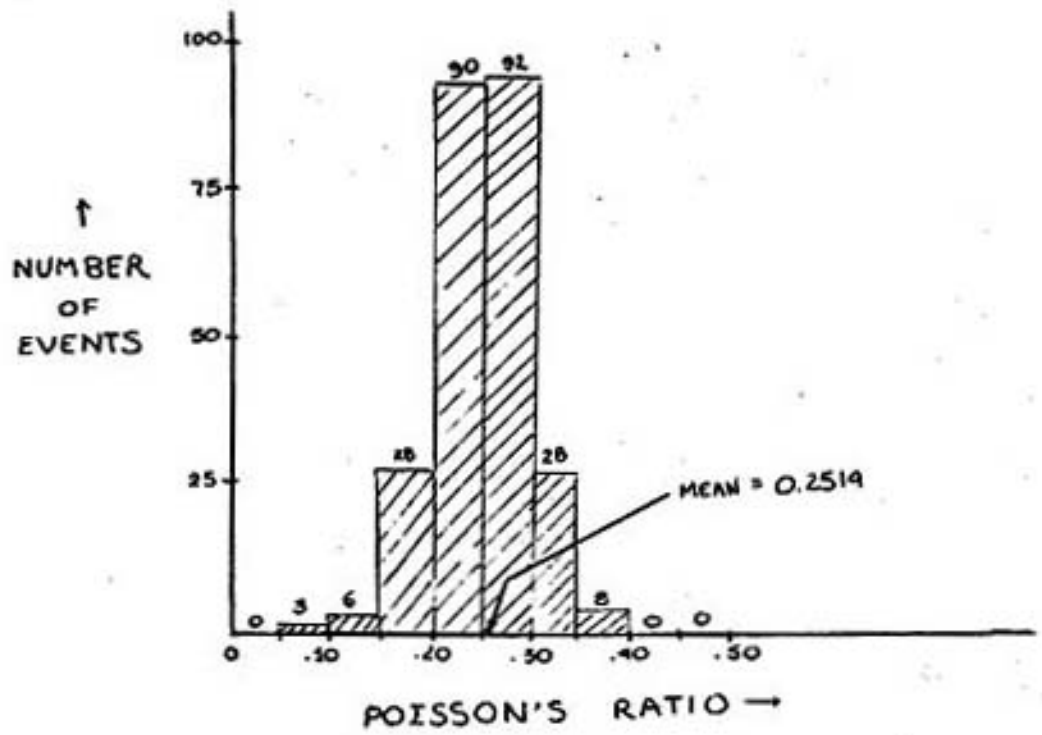

Figure 11. Diagram showing the distribution of Poisson's ratios found from the Wadati diagram analysis. Values of Poisson's ratio were grouped by increments of 0.05, where the numbers appearing above a particular block represent the number of Wadati plots yielding a value of $\sqrt{}$ within that 0.05 interval.

to define anomalous areas in the crust for the region of study. (see Figures 12-16).

VI. Results and Discussion

The average value for Poisson's ratio, obtained from the Wadati analysis, was 0.2514 with a standard deviation of 0.0516. The Poisson's ratios calculated from individual Wadati diagrams were found to be uniformly distributed about their mean (see Figure 11). This latter result assures statistical significance of the average Poisson's ratio obtained, at a one standard deviation confidence level. The average ν found by Sakdejayont (1974) and Caravella (1976) are both within one standard deviation of the result obtained in this paper

Several of the Wadati diagrams, which could not be eliminated from the analysis by any of the criteria previously mentioned, yielded unreasonably low values for Poisson's ratio (0.039 to 0.111). The five Wadati plots exhibiting this property were felt to be of importance, as unlikely values of ν are still obtained when a two standard deviation confidence interval about these values of ν is applied. The Wadati diagrams for these microearthquakes are included in Appendix A. The author believes that these anomalous Wadati plots were the result of an insufficient amount of data to effectively determine a line. No correlation between the hypocenter locations or station distributions for these anomalous diagrams was found.

The results of the composite S-P interval versus travel-time plot, discussed in Section 5 of this report, showed substantial correlation among the data. A correlation coefficient of 0.9065 was obtained for the plot, which consisted of more than 1,000 data points. This rela-

tively high correlation indicates that the travel-times were consistent with their associated S-P intervals. This provides some justification for using the travel-times to obtain values for Poisson's ratio in the spatial distribution analysis.

The final segment of this report involved the determination of spatial variations in Poisson's ratio. The raypath technique devised by Caravella (1976) and discussed in Section 6 of this paper was used to determine values of ν for crustal wedges originating from various seismograph stations. An azimuthal increment of ten degrees was chosen as the angular width of the wedges because it was felt that smaller azimuthal increments were not justified (due to hypocenter uncertainties in the microearthquake locations), and that sufficient accuracy could be attained using a ten degree width.

A total of 167 wedges were constructed from the data, using at least three points (three S-P intervals and their associated travel-times) for any ten degree sector. Of the 167 wedges, nearly 30% had Poisson's ratios greater than 0.275. In order to map areas with anomalously high Poisson's ratio, it was decided to use only those wedges whose values of ν were greater than 0.275 at the 95% confidence level, i.e. wedges whose ν's were less than 0.275 after having two standard deviations subtracted from them were not considered anomalous. This technique reduced the total number of anomalous wedges to 40. Intersections among the 40 remaining wedges were examined in order to map areas of anomalously high Poisson's ratio.

The mapping of wedges having low (<0.170), normal (0.170 to 0.274) and high (>0.275) values of Poisson's ratio was used to assure

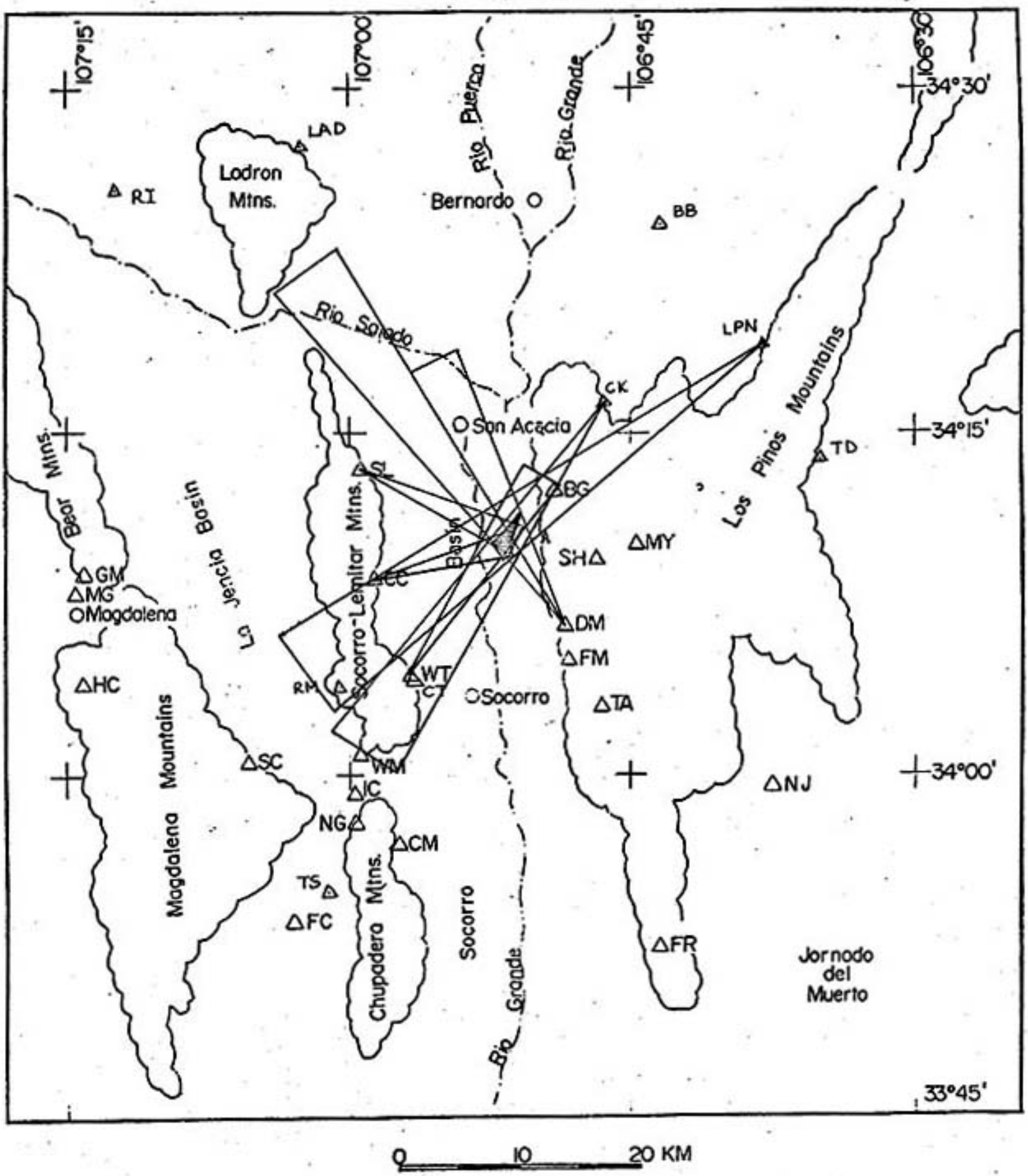

Figure 12. Anomalous area A, defined by 7 intersecting crustal wedges having Poisson's ratios of 0.275 and above at the 95% confidence level.

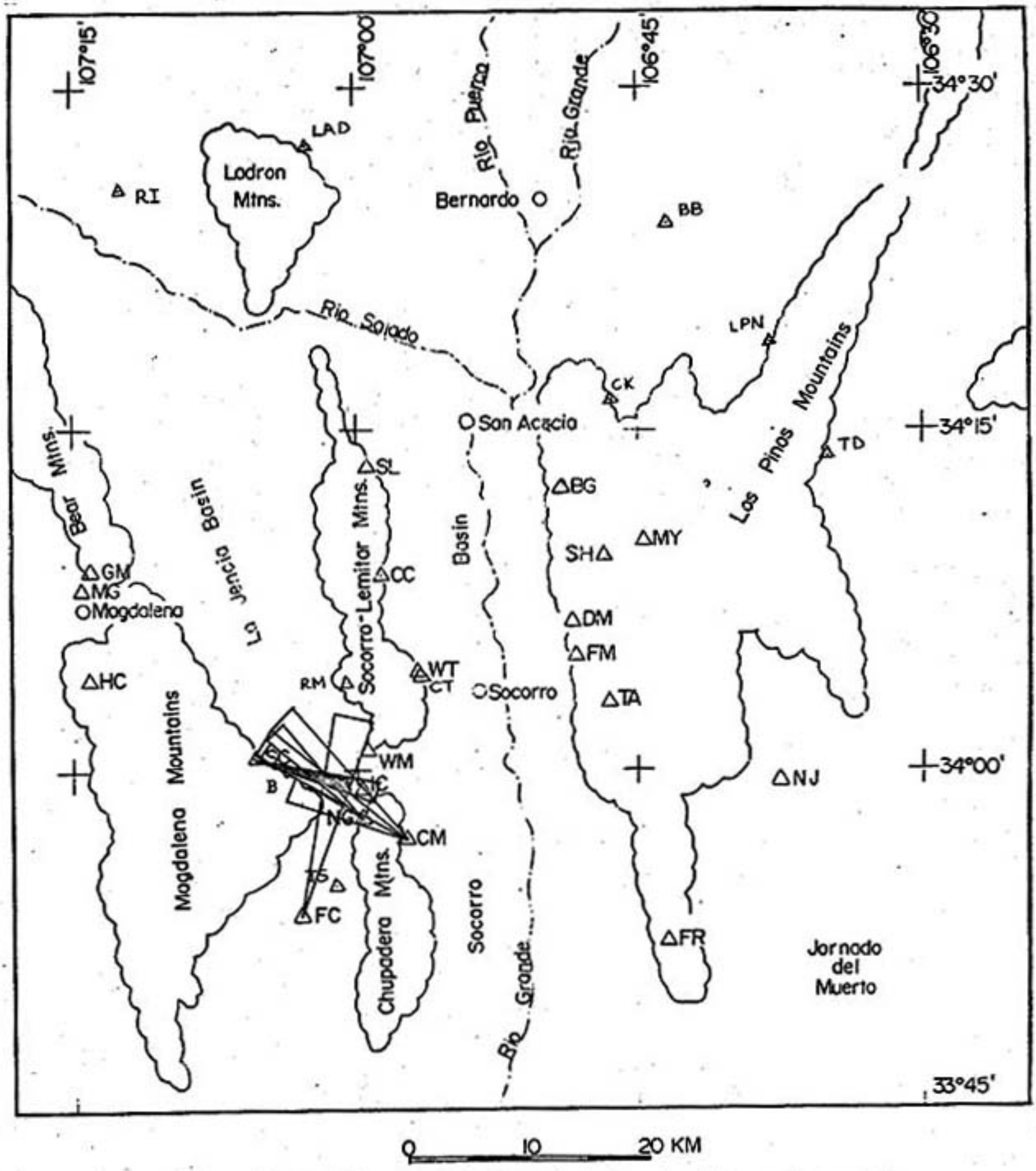

Figure 13. Anomalous area B, determined from the intersections of 6 crustal wedges having Poisson's ratio values of 0.280 and above at the 95% confidence level.

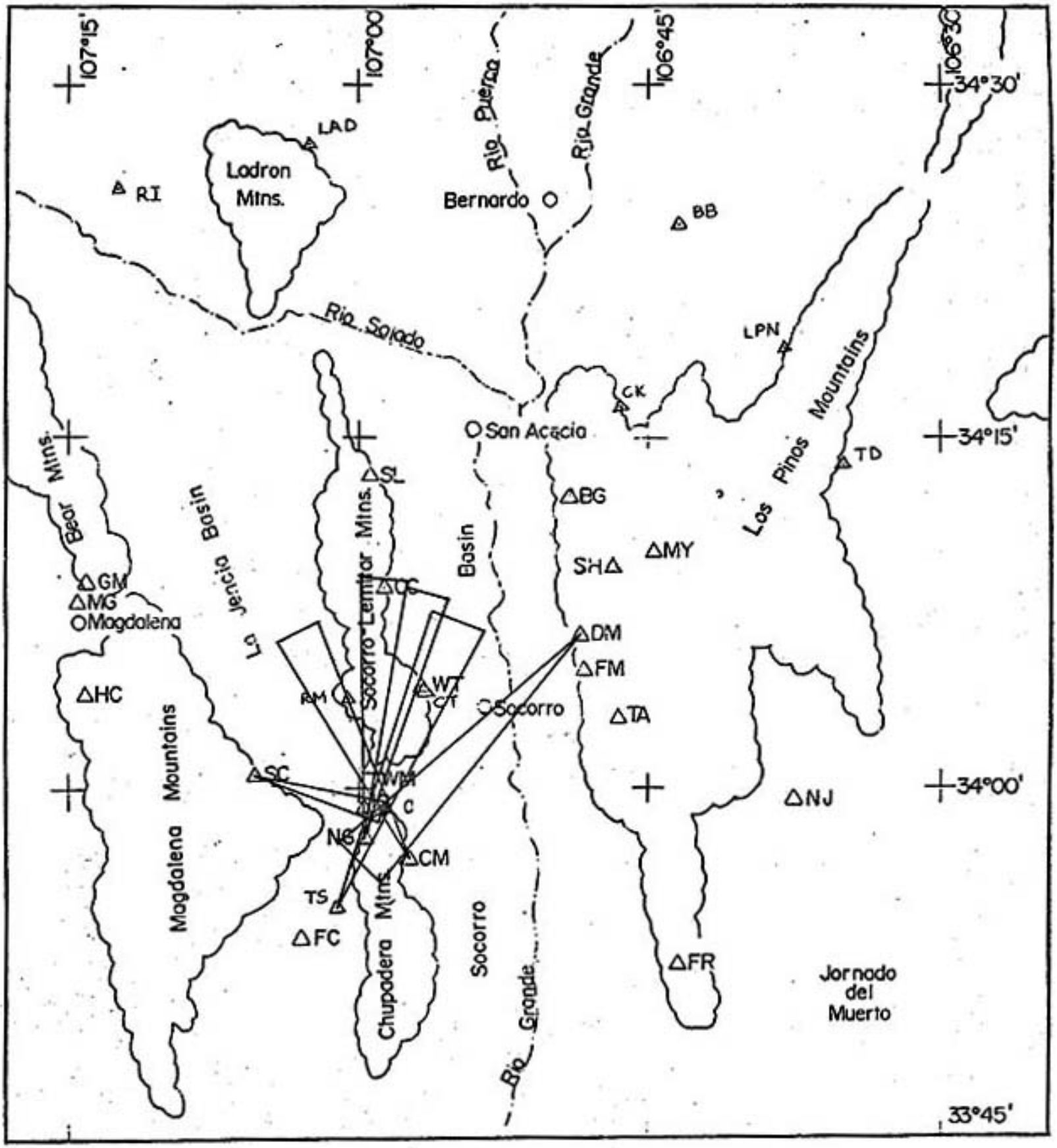

Figure 14. Anomalous area C, determined by 6 crustal wedges having values of Poisson's ratio of greater than 0.279 at the 95% confidence level.

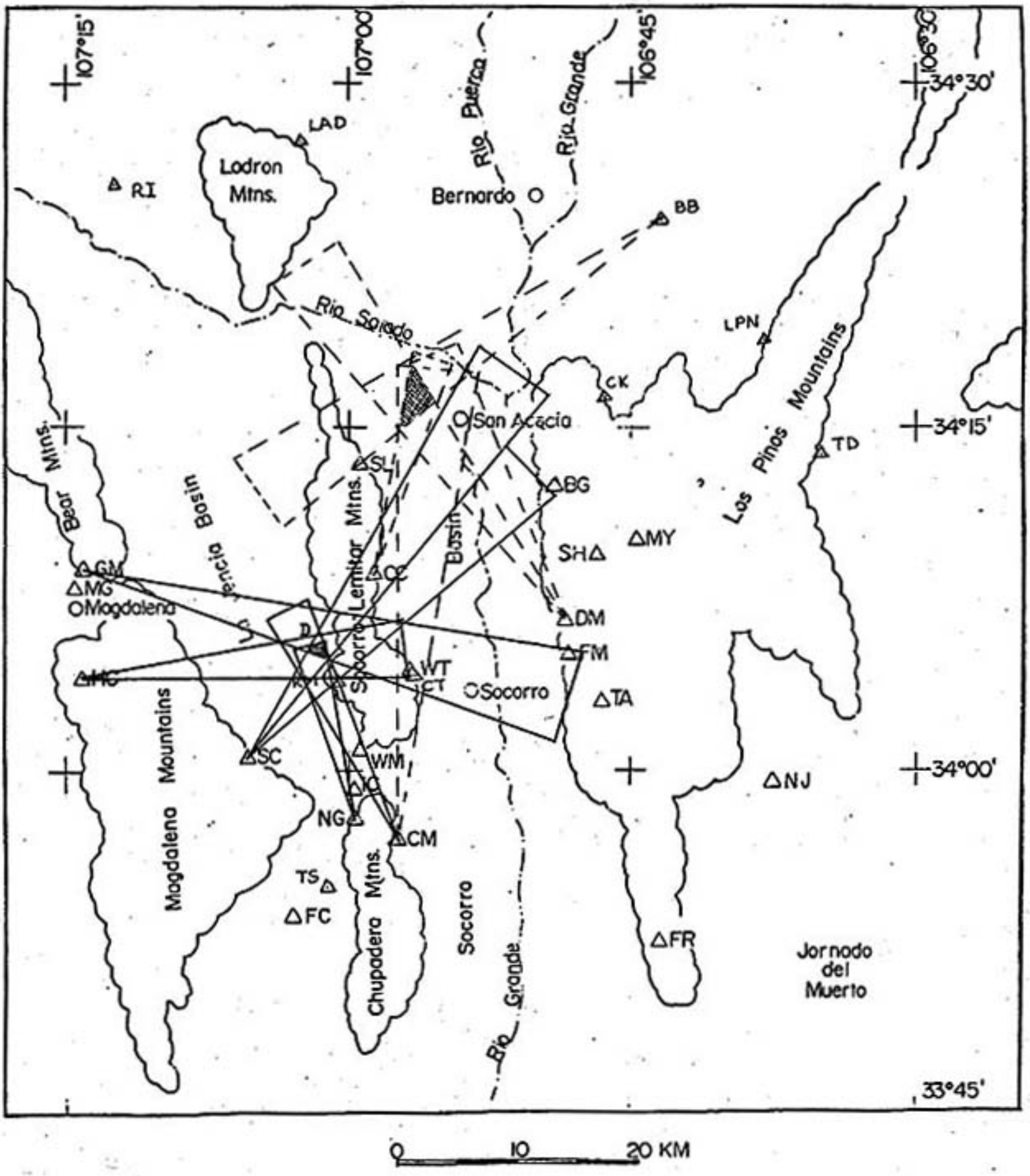

Figure 15. Anomalous area D and anomalous area that cannot be supported by this report. Area D was determined from 6 wedges having Poisson's ratios of 0.275 or greater at the 95% confidence level.

consistency between the data and the locations of anomalous areas of Poisson's ratio, and to provide control for determining the size and shape of those areas. The rule followed in the mapping procedure was to explain the maximum number of anomalous crustal wedges with the least number of anomalous areas. The results of this analysis are shown in Figures 12-16.

A total of 5 areas of anomalous Poisson's ratio was determined using intersections of four or more crustal wedges having Poisson's ratios exceeding 0.275 at the 95% confidence level. When crustal wedges of both normal and low values of ν were added to the analysis, only 4 of the 5 areas of anomalous Poisson's ratio could be supported. These four areas, labled A, B, C, and D in Figures 12-16, can be used to explain all but three of the anomalous crustal wedges obtained in this study.

Anomalous area A (Figure 12) was located using seven intersecting crustal wedges having Poisson's ratios greater than 0.275 at the 95% confidence level. The seismograph stations from which these wedges originated were CC, CK, DM, SL and WT, with two adjacent wedges from DM. The size and shape of area A was established by using the above seven wedges and crustal wedges of normal and low Poisson's ratio from stations BG, CC, CK, KY, LAD and WT. Additional crustal wedges exhibiting anomalously high, normal, and low values for ν could have been used in locating area A, however their addition would not have altered any of the boundaries already determined, and would merely duplicate the existing information. Such extraneous crustal wedges will henceforth not be mentioned.

The second region of anomalously high Poisson's ratio determined by this study is located along the southern margin of the La Jencia basin, approximately 3 km west of station IC. The intersections of six crustal wedges having Poisson's ratios in excess of 0.280 at the 95% confidence level were used to determine this area (denoted B, in Figure 13). Wedges having normal to low values of Poisson's ratio from stations CM, HC, NG, SC, WM and WT were used to establish the boundaries of area B while stations CM, FC, NG, and SC were the sources of the six anomalous wedges. The region shown in Figure 13 could consist of several smaller areas having anomalously high Poisson's ratios, as proposed by Johnston (1978) and Wallace (1978) (see Figures 17 and 18), however the crustal wedge approach adopted in this paper is not able to resolve such fine detail. Area B is the largest anomalous region found in this study, with an areal extent of nearly 20 km^2.

A third anomalous area, determined by six intersecting crustal wedges having Poisson's ratios greater than 0.279 at the 95% confidence level, is located along the northern tip of the Chupadera Mountain Block, approximately 1 km east of seismograph station IC (Area C, Figure 14). This region was determined by anomalous wedges originating from stations CM, DM, NG, SC and TS, and was bounded by crustal wedges having normal to low values of Poisson's ratio from stations CM, DM, NG, SC and WT. Area C might have been better resolved if data had been available to construct crustal wedges crossing the anomaly from seismic stations IC and WM.

The final area of anomalously high Poisson's ratio that can be sup-

ported by this study is located approximately 4 km north-west of station RM (Region D; Figure 15). Six wedges having Poisson's ratios of 0.275 or above at the 95% confidence level were drawn from seismograph stations CM, GM, HC, NC and SC to obtain region D. The boundaries of area D were primarily determined by crustal wedges having normal values of Poisson's ratio from from stations GM, IC and WT. An absence of earthquake epicenters (see Figure 4) is associated with this region, which might indicate a relatively shallow anomaly (Sanford, personal communication, 1978).

A fifth area defined by intersections of five crustal wedges having Poisson's ratios of 0.275 Or greater at the 95% confidence level is shown in Figure 15. This area is located approximately 6 km northeast of station SL. The author felt that the anomalous wedges from stations DM and CM, used to locate the area, have already been explained by regions A and C, and thus should not be used to resolve an additional anomalous area. The two remaining wedges from CC and BB, which have Poisson's ratios of 0.286 and 0.281 at a 95% confidence level respectively, can not be explained either by reading error or a lack of sufficient data. The intersecting wedges from stations BC, CK, SL, LAD and LPN all have normal to low values of Poisson's ratio. The small amount of corraborating evidence combined with the disagreement among the data was felt to be sufficient grounds for not defining an anomalous region in this area.

As was stated previously, all but three of the anomalous crustal wedges found in this study could be explained by the four areas discussed above. The two anomalous wedges from stations BB and CC have

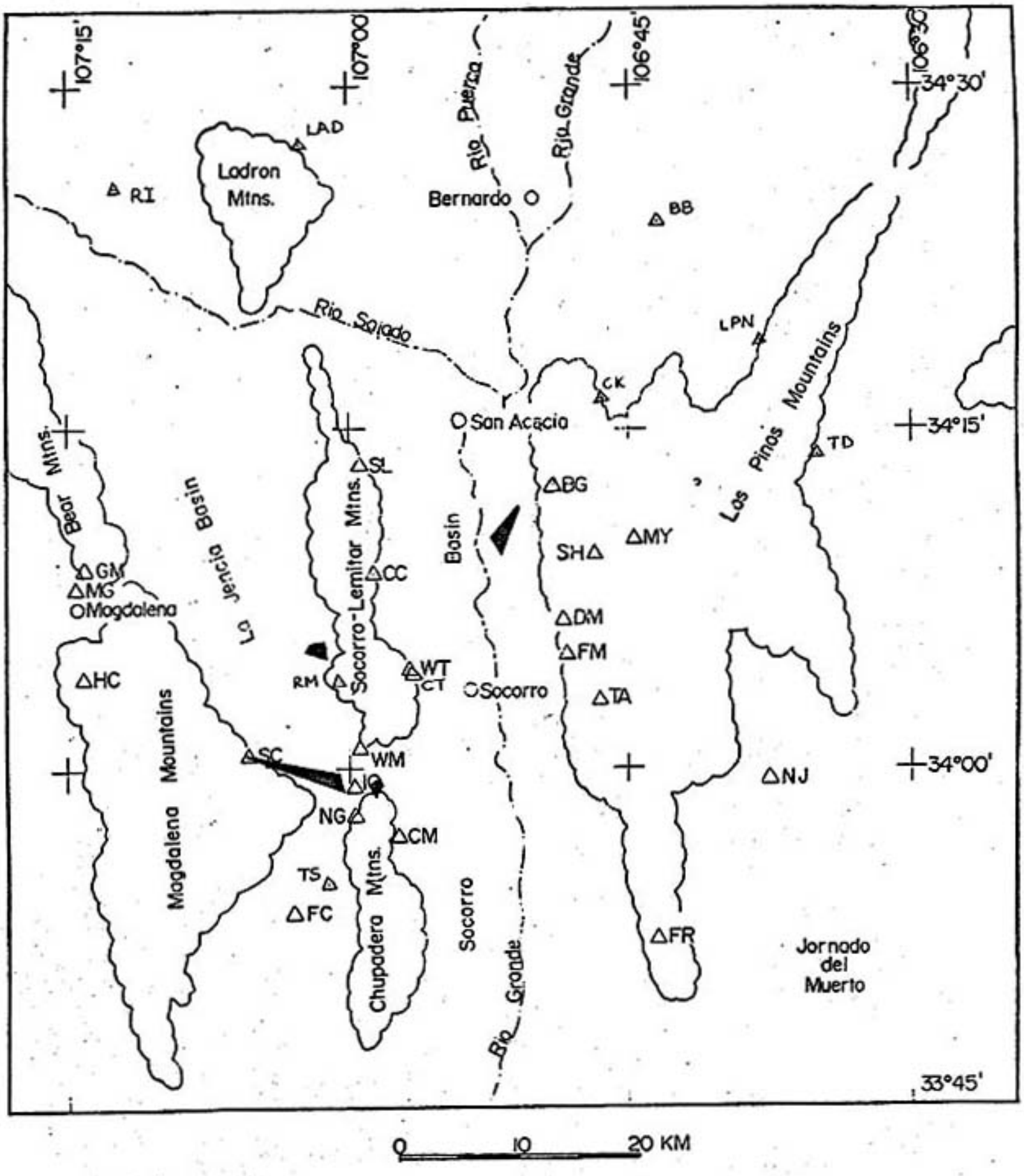

Figure 16. Map showing the four regions of anomalously high (> 0.275 at the 95% confidence level) Poisson's ratio determined in this study.

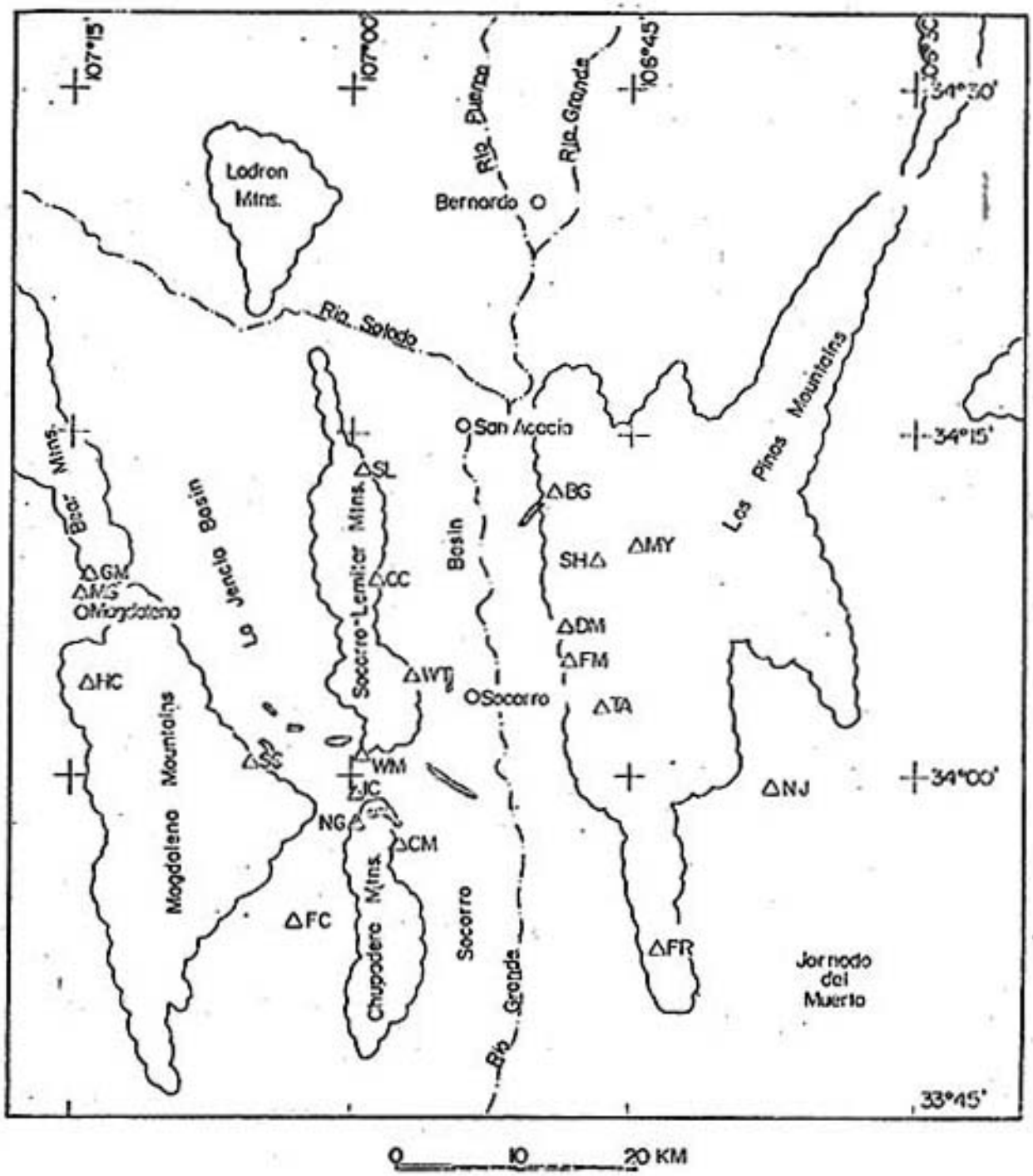

Figure 17. The positions of the eight proposed attenuating volumes of crustal rock relative to the physiographic features of the Socorro area (from Johnston (1978)).

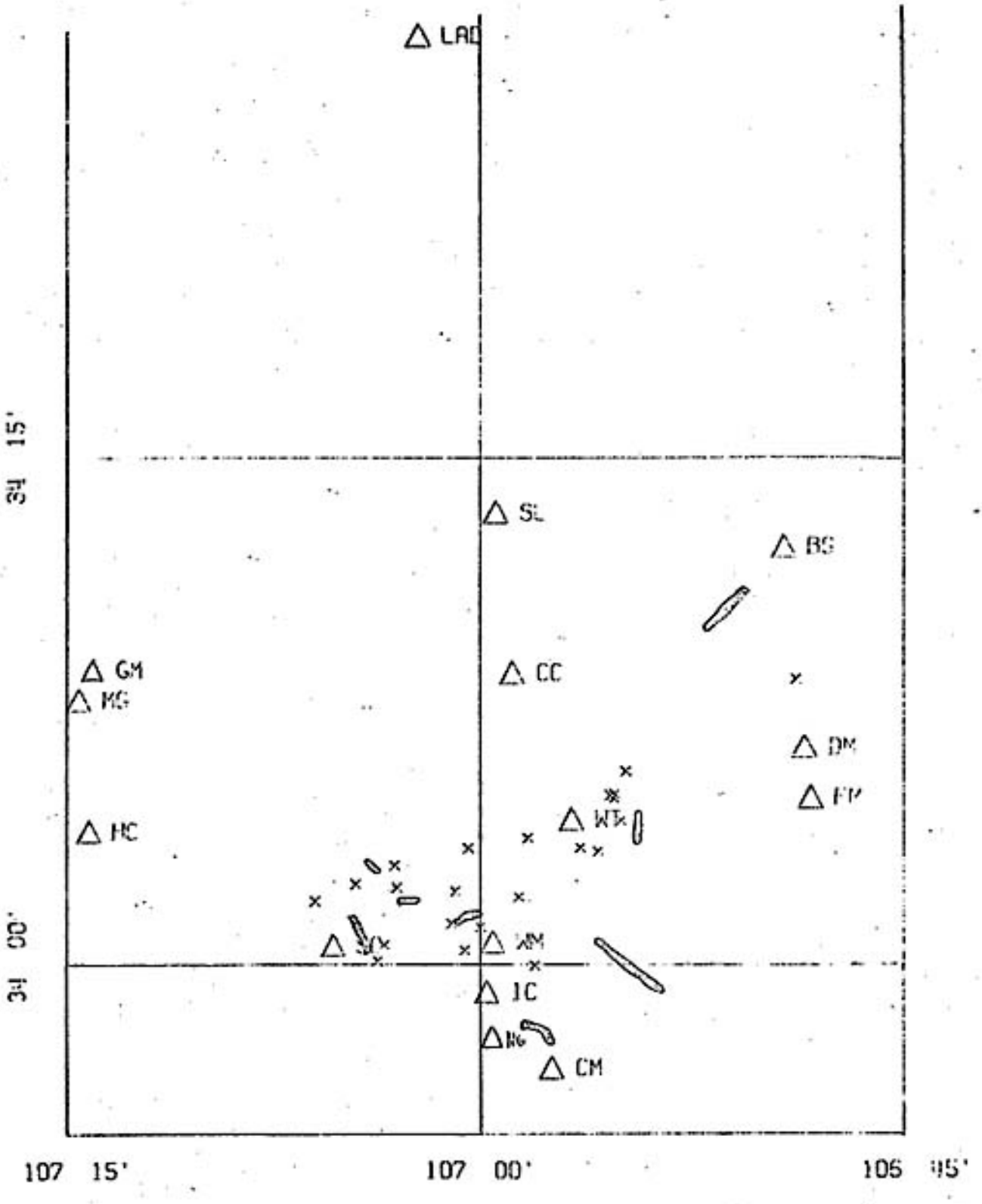

Figure 18. The positions of the eight proposed crustal volumes relative to the microearthquake swarms located by Wallace (1978).

already been mentioned. The final unexplained crustal wedge, which has a Poisson's ratio of 0.281 at the 95% confidence level, is the 50-60 degree sector from station CM. There are no other crustal wedges (anomalous or normal) that intersect this wedge, and no errors in the measurements or analysis were found. The shallow magma body proposed by Johnston (1978), located to the northeast of station CM, could explain the high value of Poisson's ratio obtained for this crustal wedge, but this proposed anomaly is not able to be supported by this study.

Figure 16 displays the four anomalous areas, determined by this report, on a single map so that the results of the studies of Caravella (1976), Johnston (1978) and Wallace (1978) may be more easily compared.

VII. Conclusions

The average value for Poisson's ratio for the upper crust in the Socorro, New Mexico area is 0.251 ± 0.052. Localized areas of anomolously high Poisson's ratio (0.275 at the 95% confidence level) exist, and may be spatially mapped using body wave arrivals from microearthquakes.

The method of determining the spatial distribution of Poisson's ratio using crustal wedge intersections provides an excellent indirect procedure for mapping anomalous areas of Poisson's ratio. Smaller azimuthal increments and larger data sets could be employed in future studies to obtain a more detailed spatial distribution.

References Consulted

Aki, Keiiti(1976). Determination of Three-Dimensional Velocity Anomalies Under a Seismic Array Using First P Arrival Times From Local Earthquakes, Jour. of Geophysical Res., 81, 4381-4399.

Bullen, K.E.(1963). An Introduction to the Theory of Seismology, Cambridge University Press, London, England.

Caravella, Frank J.(1976). A Study of Poisson's Ratio in the Upper Crust in the Socorro, New Mexico, Area, M.S. Independent Study, Geoscience Department, N.M.I.M.T.

Chapin, C.E. and W.R. Seager(1975). Evolution of the Rio Grande Rift in the Socorro and Las Cruces Area, in New Mexico Geol. Society Guidebook, 26th Field Conference, 297-321.

Chapin, C.E., R.M. Chamberlain, G.R. osburn, D. White, and A.R. Sanford(1978). Exploration Framework of the Socorro Geothermal Area, New Mexico, Special Publication no. 7, 115-130.

Draper, Norman and Harry Smith(1966). Applied Regression Analysis, John Wiley & Sons Inc., N.Y., N.Y., 77-85.

Johnston, J.A.(1978). Microearthquake Frequency Attenuation of S Phases in the Rio Grande Rift Near Socorro, New Mexico, M.S. Independent Study, Geoscience Dept., N.M.I.M.T.

Nettleton, L.L.(1940). Geophysical Prospecting for Oil,McGraw-Hill Book Company, N.Y., N.Y., 236-237.

Reilinger, R. and J.E. Oliver(1976). Modern Uplift Associated With a Proposed Magma Body in the Vicinity of Socorro, New Mexico, Geology, 4, 583-586.

Reiter, M. and R. Smith(1977). Subsurface Temperature Data in the Socorro Peak KGRA, New Mexico, Geothermal Energy Magazine, 5, 37-41.

Rinehart, E.J.(1976). The Use of Microearthquakes to Map an Extensive Magma Body in the Socorro, New Mexico Area, M.S. Independent Study, Geoscience Department, N.M.I.M.T.

Rinehart, E.J.(1978). Abstract submitted for 1978 International Rift Symposium, Sante Fe, New Mexico.

Sakdejayont, K.(1974). A Study on Poisson's Ratio and V_p/V_s Ratio in the Rio Grande Rift, M.S. Independent Study, Geoscience Department, N.M.I.M.T.

Sanford, A.R. and C.R. Holmes(1962). Microearthquakes Near Socorro, New Mexico, Journal of Geophysical Research, 67, 4449-4459.

Sanford, A.R. and L.T. Long(1965). Microearthquake Crustal Reflections, Bull. Seismo. Soc. of Amer., 55, 579-586.

Sanford, A.R.,O. Alptekin, and T.R. Toppozada(1973). Use of Reflection Phases on Microearthquake Seismograms to Map an Unusual Discontinuity Beneath the Rio Grande Rift, Bull. of Seismol. Soc. of Amer., 63, 2021-2034.

Sanford, A.R., R.P. Mott, Jr., P.M. Shuleski, E.J. Rinehart, F.J. Caravella, R.M. Ward, and T.C. Wallace(1977). Geophysical Evidence for a Magma Body in the Crust in the Vicinity of Socorro, New Mexico, Amer. Geop. Union, Geo. Mono. #20, 385-403.

Shuleski, P.J.(1976). Seismic Fault Motion and SV-Wave Screening by Shallow Magma Bodies in the Vicinity of Socorro, New Mexico, M.S. Independent Study, Geoscience Department, N.M.I.M.T.

Wallace, T.C.(1978). Microearthquake Swarm Activity in the Socorro, New Mexico Area, D.S., Geoscience Dept., N.M.I.M.T.

APPENDIX A :

Wadati diagrams which yielded unreasonably low values for Poisson's ratio

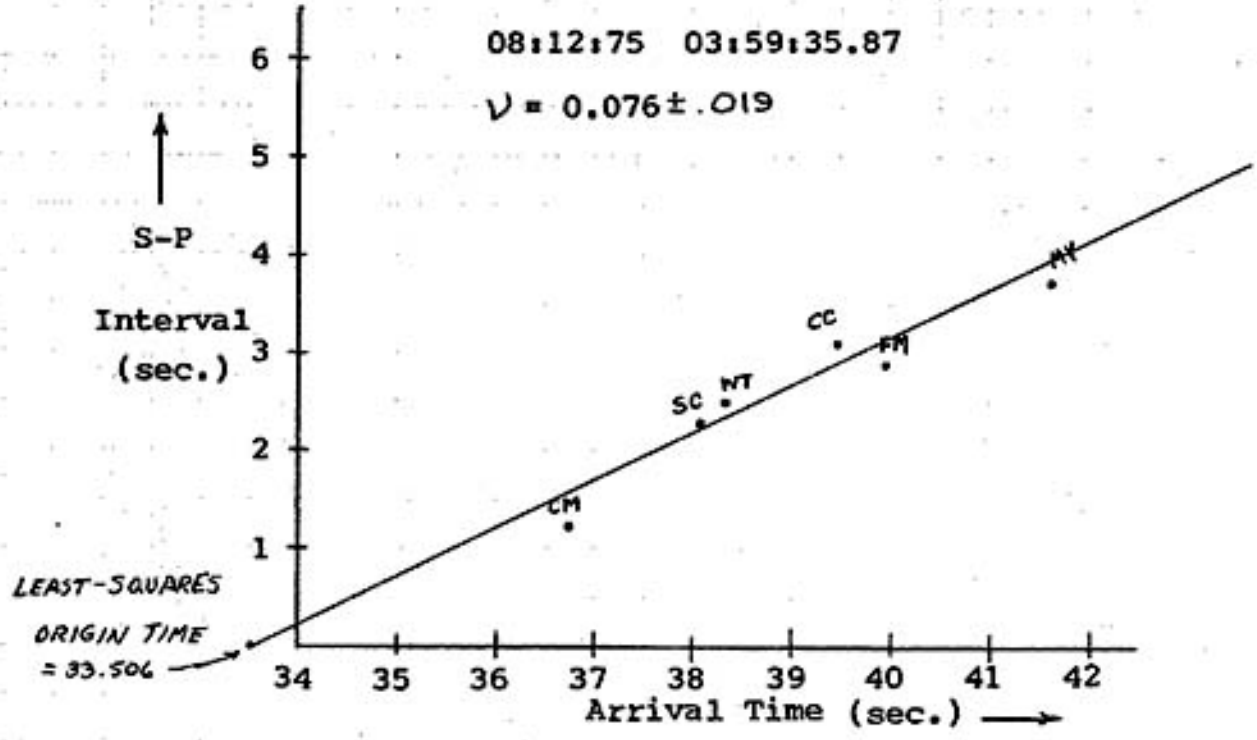
08:12:75 03:59:35.87
ν = 0.076 ± .019
S-P
Interval
(sec.)
LEAST-SQUARES
ORIGIN TIME
= 33.506
CM
SC
WT
CC
FM
MY
Arrival Time (sec.)

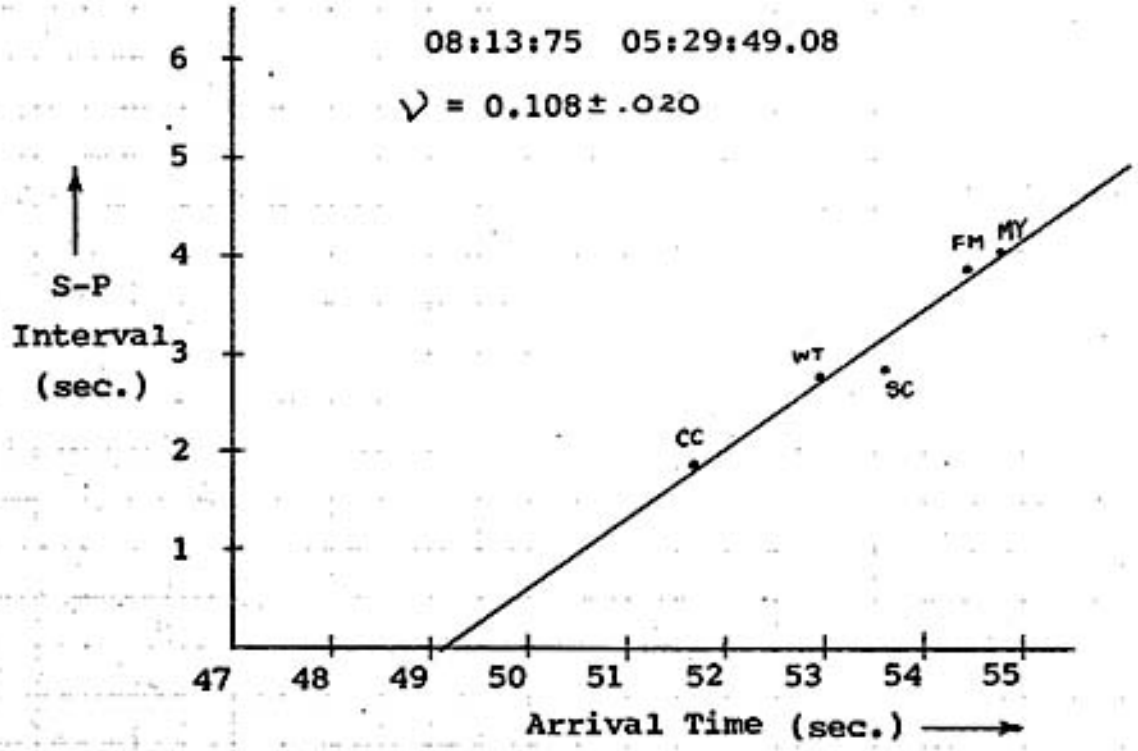
08:13:75 05:29:49.08
ν = 0.108 ± .020
S-P
Interval
(sec.)
CC
WT
SC
FM
MY
Arrival Time (sec.)

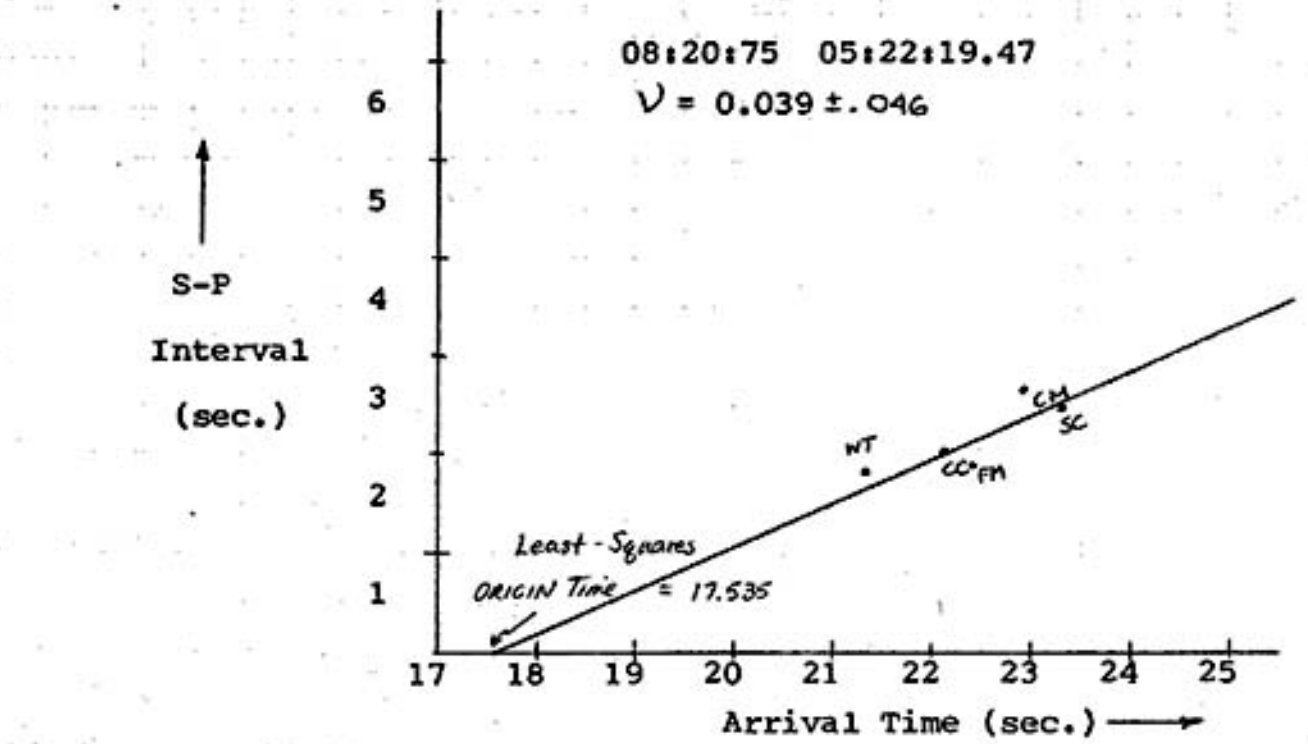
08:20:75 05:22:19.47
ν = 0.039 ± .046
S-P
Interval
(sec.)
6
5
4
3
2
1
CM
SC
WT
CC*FM
Least-Squares
ORIGIN Time = 17.535
17
18
19
20
21
22
23
24
25
Arrival Time (sec.) ⟶

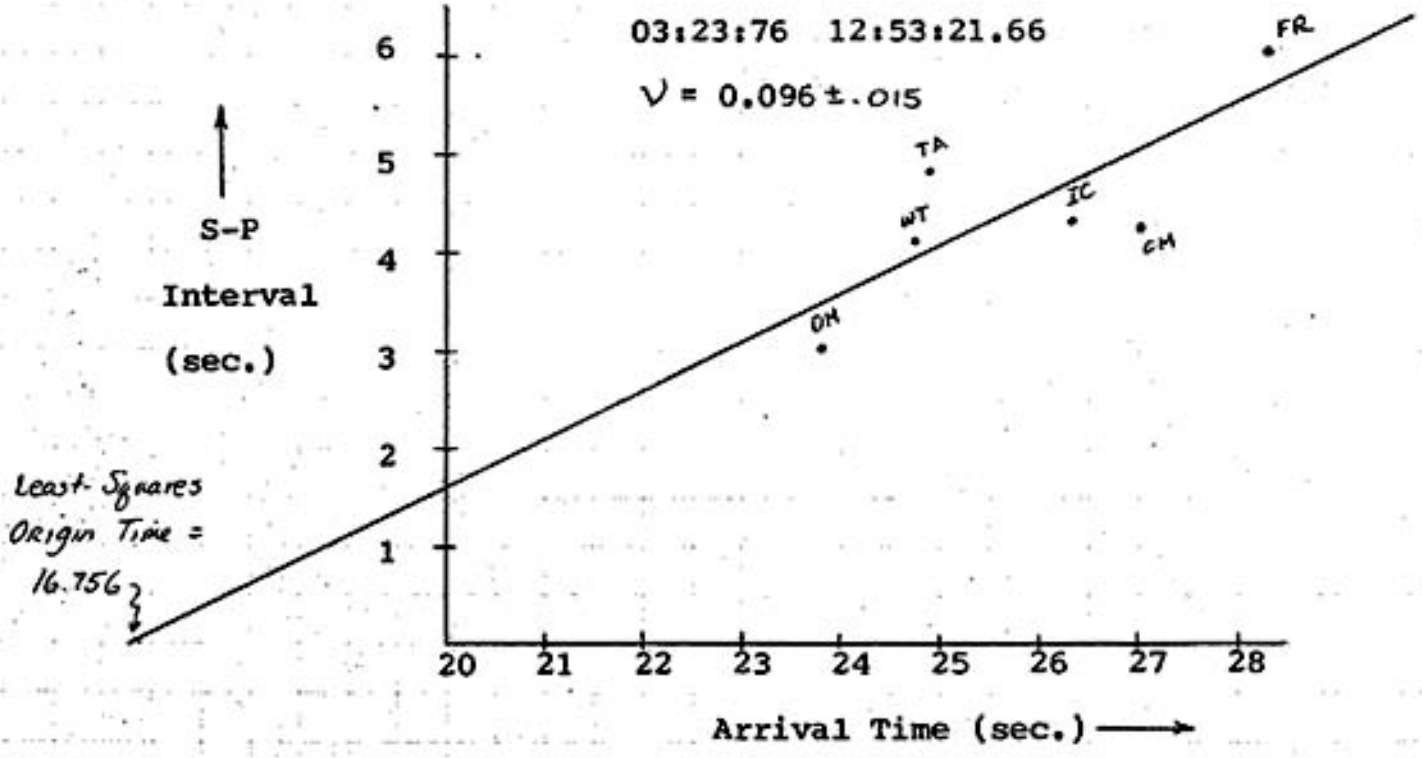
03:23:76 12:53:21.66
ν = 0.096 ± .015
FR
TA
WT
IC
CM
OM
S-P
Interval
(sec.)
6
5
4
3
2
1
Least-Squares
Origin Time =
16.756
20
21
22
23
24
25
26
27
28
Arrival Time (sec.) ⟶

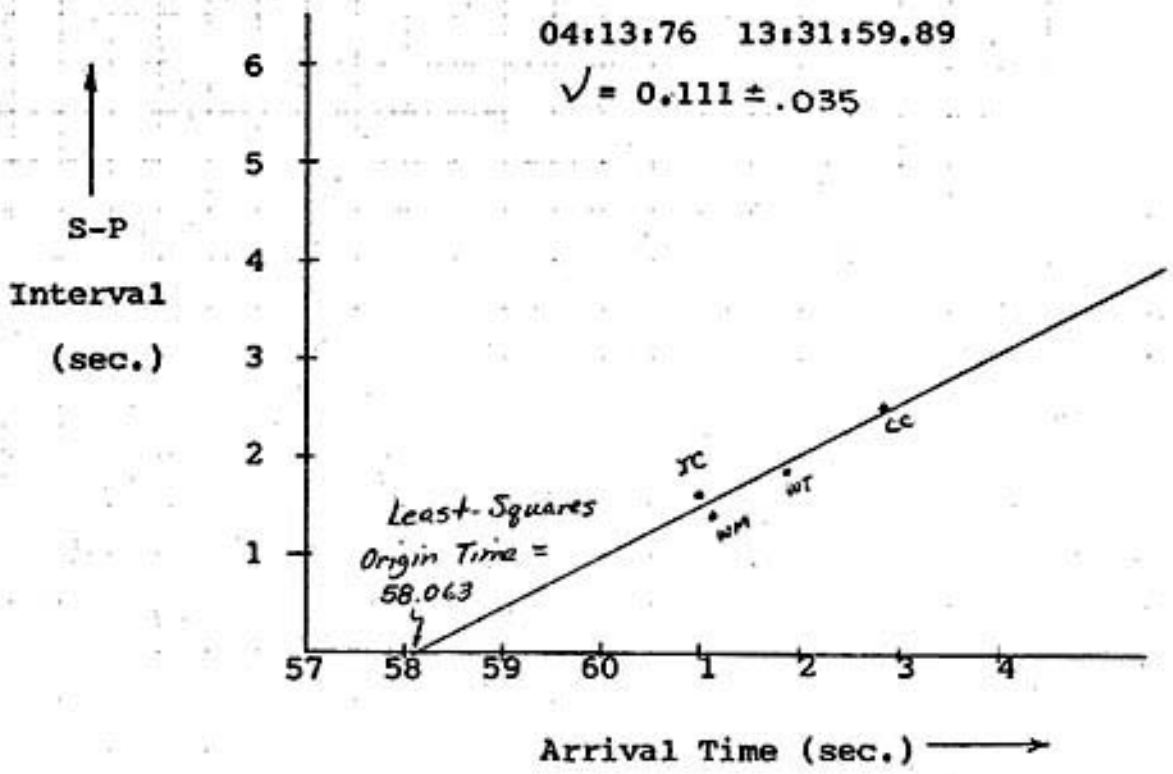
04:13:76 13:31:59.89
√ = 0.111 ± .035
S-P
Interval
(sec.)
6
5
4
3
2
1
Least-Squares
Origin Time =
58.063
JC
WM
WT
CC
57
58
59
60
1
2
3
4
Arrival Time (sec.)